SEMMELWEIS EGYETEM

DOKTORI ISKOLA

Ph.D. értekezések

2912.

PATÓ ANNA TERÉZIA

Celluláris és molekuláris élettan
című program

Programvezető: Dr. Hunyady László, egyetemi tanár

Témavezető: Dr. Sirokmány Gábor, egyetemi docens

ROLE OF DUAL OXIDASE 1 IN SQUAMOUS CELLS

Ph.D. thesis

Anna Terézia Pató, M.D.

Doctoral School of Molecular Medicine

Semmelweis University

Supervisor: Gábor Sirokmány, M.D., Ph.D.

Official reviewers: Csaba Sőti, M.D., D.Sc.

Szilvia Benkő, Ph.D.

Head of the Complex Examination Committee: Zoltán Prohászka, M.D., D.Sc.

Members of the Complex Examination Committee:

László Homolya, D.Sc.

Tamás Kardon, M.D., Ph.D.

Budapest

2023

Table of Contents

List of Abbreviations

3R	replace, reduce, refine
AITC	allyl isothiocyanate
AM	acetoxymethyl ester
ATP	adenosine triphosphate
BIAM	biotin polyethyleneoxide iodoacetamide
C.elegans	Caenorhabditis elegans
CBS	cation binding sites
cDNA	complementary deoxyribonucleic acid
CE	cornified envelope
Ce-DUOX	Caenorhabditis elegans dual oxidase
CGD	chronic granulomatous disease
CH	congenital hypothyroidism
COX-2	cyclooxygenase-2
C_P	peroxidatic cysteine
CPS	composite pain score
C_R	resolving cysteine
CRISPR-Cas9	Clustered Regularly Interspaced Short Palindromic Repeats-CRISPR associated protein 9
C-terminal	carboxyl-terminus
CYBA	Cytochrome B-245 Alpha Chain
CYBB	Cytochrome B-245 Beta Chain
DCM	disseminated coccidioidomycosis
dDUOX	Drosophila dual oxidase
DH	dehydrogenase
DKO	double-knockout
DMEM	Dulbecco's modified Eagle's medium
DMSO	dimethyl sulfoxide
DNA	deoxyribonucleic acid
DPP	Dipeptidyl Peptidase
DRG	dorsal root ganglia
DSC1	desmocollin 1

DSG1	desmoglein 1
DTT	dithiothreitol
DUOX	dual oxidase
DUOXA1	dual oxidase maturation factor 1
DUOXA2	dual oxidase maturation factor 2
EEF-2	eukaryotic translation elongation factor 2
EGF	epidermal growth factor
EGFR	epidermal growth factor receptor
ER	endoplasmic reticulum
ERK	extracellular signal-regulated kinase
FAD	flavin adenine dinucleotide
FBS	fetal bovine serum
FNE	free nerve ending
GAPDH	glyceraldehyde-3-phosphate dehydrogenase
GTP	guanosine-5'-triphosphate
HRP	horseradish peroxidase
HyPer	hydrogen peroxide sensor
i.pl.	intraplantar
IAV	Influenza A virus
IFN	interferon
IL	interleukin
KO	knockout
KRT	keratin
LPO	lactoperoxidase
LPS	lipopolysaccharide
LTB4	leukotriene B4
MAPK	mitogen-activated protein kinase
MCT8	monocarboxylate transporter 8
MMP-9	matrix metalloproteinase-9
mRNA	messenger ribonucleic acid
NADPH	reduced nicotinamide adenine dinucleotide phosphate
NEM	N-ethylmaleimide

NF-κB	nuclear factor kappa-light-chain-enhancer of activated B cells
NIS	sodium/iodide symporter
NOX	NADPH oxidase
NOXA1	NADPH Oxidase Activator 1
NOXO1	NADPH Oxidase Organizer 1
N-terminal	amino-terminus
PBS	Phosphate-buffered saline
PCR	polymerase chain reaction
PGE2	prostaglandin E2
PHD	peroxidase-homology domain
PHLD	pleckstrin homology-like domain
phox	phagocyte oxidase
PMA	phorbol 12-myristate 13-acetate
PMSF	phenylmethylsulfonyl fluoride
PRR	pattern recognition receptor
Prx	peroxiredoxin
PTP	protein tyrosine phosphatase
qPCR	quantitative polymerase chain reaction
Renox	renal NADPH oxidase
RNA	ribonucleic acid
ROS	reactive oxygen species
SDS	sodium dodecyl sulfate
SERPINB	Serpin family B member
siRNA	small interfering ribonucleic acid
Srx	sulfiredoxin
STAT	signal transducer and activator of transcription
T3	3,5,3'-triiodothyronine
T4	3,5,3',5'-tetraiodothyronine or thyroxine
TG	thyroglobulin
TGM	transglutaminase
Th1	T helper 1
Th2	T helper 2

THOX1	thyroid oxidase 1
THOX2	thyroid oxidase 2
TKO	triple-knockout
TLR	Toll-like receptor
TM	transmembrane
TNF	tumor necrosis factor
TPO	thyroid peroxidase
TRIF	TIR-domain-containing adapter-inducing interferon-β
TRP	transient receptor potential
TRPA	transient receptor potential ankyrin
TRPM	transient receptor potential melastatin
TRPV	transient receptor potential vanilloid
Trx	thioredoxin
TrxR	thioredoxin reductase
VEOIBD	very early-onset inflammatory bowel disease

1. Introduction

Reactive oxygen species (ROS) refer to unstable oxygen derivatives, including superoxide ($O_2^{\bullet -}$), hydrogen peroxide (H_2O_2), and hydroxyl radical ($OH^{\bullet}$), among others (1). These molecules can be produced in living organisms in a non-regulated way through lipid metabolism within the peroxisomes, cyclooxygenases, as well as mitochondrial oxidative metabolism (2). Previously considered as harmful metabolic by-products, ROS have now been recognized to play a role in various physiological processes, such as host defense and hormone biosynthesis, when generated under controlled conditions. Members of the NOX NADPH oxidase family are the primary source for regulated production of ROS in mammalian cells (3).

1.1 Mammalian NADPH oxidases

Mammalian NADPH oxidases, namely NOX1-5 and DUOX1-2, are membrane-integrated enzymes that utilize NADPH and FAD to transport an electron across the membrane, to reduce molecular oxygen into superoxide, as described by the following reaction:

$$NADPH + 2O_2 \rightarrow NADP^+ + 2O_2^{\bullet -} + H^+$$

Superoxide is then rapidly, spontaneously or enzymatically, converted to hydrogen peroxide. The NOX/DUOX enzymes share similar structure and possess a highly conserved catalytic core consisting of six transmembrane (TM) α-helical domains, including two heme B prosthetic groups responsible for transferring electrons from NADPH-FAD through the membrane. In addition, all isoforms comprise dehydrogenase (DH) domain with FAD-binding sites followed by NADPH-binding sites located at the cytosolic C- terminus.

Additionally, DUOX enzymes contain an N-terminal, extracellular peroxidase-homology domain, an additional α-helical TM region, and two calcium-binding EF-hand motifs located on the intracellular loop between the first and second transmembrane domains. NOX5 also contains four EF-hand motifs (Figure 1.).

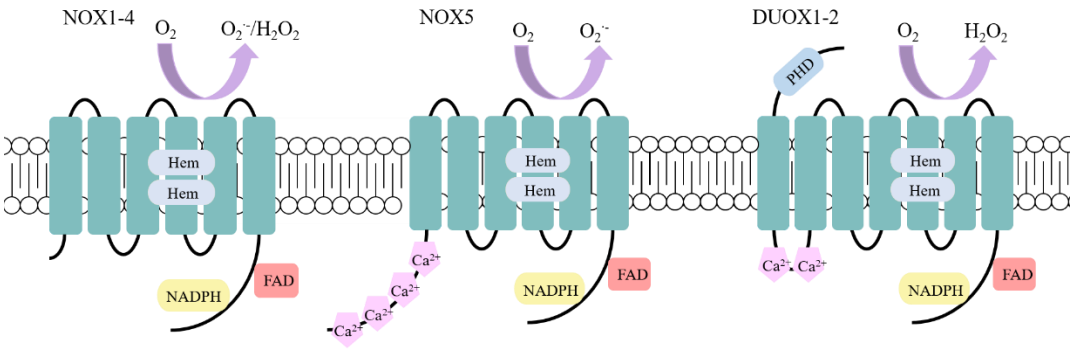

Figure 1. Domain structure of mammalian NADPH oxidases. *NOX/DUOX enzymes contain six (seven for DUOX1-2) TM domains, along with heme prosthetic group and binding sites for FAD and NADPH. In addition, the NOX5 and DUOX enzymes also possess calcium-binding EF-hand domains. (PHD: peroxidase-homology domain). The figure is based on Figure 1. of (4).*

Several NADPH oxidases function as protein complexes. The enzyme activity of NOX1-3 is regulated by their cytosolic subunits, while NOX4 appears constitutively active. DUOX enzymes and NOX5 can be stimulated by calcium. However, Dual Oxidases also require maturation factors for proper function. The presence of at least one of the NOX/DUOX enzymes has been described in almost all organs, most isoforms have a characteristic tissue distribution, and in many cases, they play well known physiological roles. For example, the importance of NOX2 in host defense or the crucial role of DUOX2 in synthesizing thyroid hormone is undisputed. However, several unanswered questions remain about their function (4-6). The NADPH oxidase enzyme family members are described in more detail below.

1.1.1 NOX2

NOX2, also known as $gp91^{phox}$ or phagocyte oxidase, is the first identified and most extensively studied NADPH oxidase isoform. The human and mouse NOX2 gene, *CYBB* is located on the X chromosome (Xp21.1). The enzyme is a 570-amino-acid-long, highly glycosylated protein, which is abundantly present in phagocytes and contributes to eliminating microorganisms. However, it is also expressed in other cells, such as neurons, cardiomyocytes, skeletal and smooth muscle cells, hepatocytes, endothelial cells, and hematopoietic stem cells. The phagocyte oxidase functions as a protein complex and requires six subunits for proper enzyme activity. Namely, $gp91^{phox}$ (NOX2), $p22^{phox}$,

p47^{phox}, p67^{phox}, p40^{phox}, and Rac. The gp91^{phox} subunit represents the catalytic core for electron transport, while p22^{phox} stabilizes NOX2 and binds to the organizer subunit, p47^{phox}. The p67^{phox} subunit acts as an activator, p40^{phox} is a regulator subunit, and Rac is a GTP-binding protein. (4, 7). Mutations in any of the subunits of the phagocyte oxidase complex can impair superoxide production, leading to chronic granulomatosis disease (CGD) and recurrent catalase-positive bacterial infections in patients (8, 9).

1.1.2 NOX1

NOX1 enzyme was the first homolog of the NOX2 to be identified (10). The human and mouse *NOX1* are also located on the X chromosome (Xq22). The 564-amino-acid-long protein is roughly 60% identical to NOX2 and generates superoxide. Furthermore, functional similarities between these two NADPH oxidase isoforms have been observed. Like phagocyte oxidase, NOX1 also necessitates additional cytosolic regulatory proteins to function. NOXO1 (NOX Organiser 1) and NOXA1 (NOX Activator 1), homologs of p47^{phox} and p67^{phox} are required, as well as p22^{phox}, stabilizer of NOX1 and the GTP-binding protein, Rac1. *NOX1* is highly expressed in colon epithelial cells. However, it is also found in many other organs and cell types, such as uterus, placenta, prostate, vascular smooth muscle cells, endothelial cells, osteoclasts, retinal pericytes, as well as in several colorectal tumor cell lines (Caco-2, DLD-1 and HT-29) and a pulmonary epithelial cell line (A549) (4, 7). The role of NOX1 is not yet fully understood, but its expression in the colon and structural similarity to NOX2 suggest involvement in host defense and gut microbiota homeostasis. In several patients, *NOX1* loss-of-function mutations have been linked to very early-onset inflammatory bowel disease (VEOIBD), although these rare mutations do not cause highly penetrant Mendelian disease (11, 12). Knockout (KO) of *Nox1* alone did not cause obvious phenotypic changes in mice. However, in mice, the absence of glutathione peroxidases-1 and -2 can lead to spontaneous ileocolitis, with the severity of the disease varying based on the mouse's genetic background. When these mice were bred to be triple-knockouts (TKO) with the addition of *Nox1* gene deletion, they displayed almost no signs of disease (e.g., lethargy and perianal alopecia). The slower growth rate and shortened small intestine observed in the double-knockout (DKO) mice were also eliminated in the TKO animals. These findings suggest that NOX1 is responsible for the ileocolitis observed in the DKO mice (13). Conversely, the combined deficiency of *Nox1* and *IL-10* in mice led to intestinal inflammation (14).

1.1.3 NOX3

Human *NOX3* is located on chromosome 6 (6q25.1-26). The 568-amino-acid-long protein is 58% identical to NOX2 and shares high similarity with NOX1 as well (7). NOX3 was identified in 2000 (15), but the first study on its function in mice was published four years later. Paffenholz *et al.* studied head-tilt mice with balance defects when they identified a lack of NOX3 behind the vestibular dysfunction (16). *NOX3* is mainly expressed in the inner ear, including the cochlear and vestibular sensory epithelia, and it is essential for the formation of otoconia crystals (16, 17). The functional enzyme complex is composed of NOX3, $p22^{phox}$, NOXO1, NOXA1, and Rac. Mutations in *Noxo1* and $p22^{phox}$-encoding *Cyba* also led to balance defects in mice. Interestingly, vestibular dysfunction was not observed for loss of function mutations in *Noxa1*. While the absence of NOX3 in mice is well characterized, no *NOX3* mutation has been described in humans, and no balance defects have been found in mutations in *CYBA*, which encodes $p22^{phox}$ (4).

1.1.4 NOX4

NOX4 is highly expressed in the kidney, where it was initially discovered and referred to as renal NADPH oxidase (Renox) (18, 19). It has since been described in several different cell types, such as osteoclasts, endothelial cells, vascular smooth muscle cells, fibroblasts, cardiomyocytes, skeletal muscle cells, adipocytes, neurons, microglia, keratinocytes, and melanoma cells. Unlike NOX1 and NOX3, which are highly similar to phagocyte oxidase, NOX4 is distantly related and shares only about 39% amino acid identity with NOX2. *NOX4* is located on chromosome 11 (11q14.2-q21) and encodes a 578 amino-acid-long membrane protein. The constitutively active H_2O_2-producing enzyme complex consists of NOX4 and $p22^{phox}$. The role of NOX4 is an intensively researched area extending beyond the kidney. NOX4-deficient mice do not display striking phenotypic differences. The function of the enzyme in the kidney, heart, lung, osteoclasts, and the development of neurodegenerative diseases has been investigated, but a clear picture has yet to emerge (4, 7, 14).

1.1.5 NOX5

NOX5 was described in 2001 (20, 21). Bánfi *et al.* identified two NOX5 isoforms (spleen, NOX5α and testis, NOX5β) and two additional splice variants such as NOX5γ and NOX5δ. These isoforms possess an extended intracellular NH_2-terminus containing four

EF-hand domains. These domains are responsible for stimulating the enzyme's superoxide production through calcium (20). Cheng *et al.* identified the fifth NOX5 isoform (NOX5ε or NOX5-S), which is not containing a calcium-binding motif (21). The human *NOX5* is located on chromosome 15 (15q22.31) and is expressed in spleen, testis, lymph nodes, ovaries, placenta, uterus, various fetal tissues, pancreas, bone marrow, and vascular smooth muscle. Unlike the other NADPH oxidase isoforms, the superoxide production of NOX5 does not require additional proteins. In addition to the increase in intracellular calcium levels, post-translational modification, and phosphorylation, among other factors, seem to stimulate the enzyme activity. The physiological role of NOX5 is poorly understood, partly due to the absence of the enzyme in rodents. NOX5 has been extensively researched by various groups in the context of cardiovascular diseases. These studies have implicated NOX5 in the pathogenesis of atherosclerosis and myocardial infarction, among others (22). Recently, Petheő *et al.* conducted a study using CRISPR-Cas9 to generate NOX5-deficient rabbits. Although there were no obvious phenotypic differences, the absence of NOX5 increased plaque formation in the aorta under a high-cholesterol diet in rabbits. This finding suggests a protective role of NOX5 in atherosclerosis that contradicts previous publications. Therefore, further investigation is necessary to fully comprehend the function of NOX5 in cardiovascular disease (23).

1.1.6 DUOX1 and DUOX2

DUOX1 and DUOX2 share approximately 50% of amino acid identity with the phagocyte oxidase, whereas the similarity between DUOX1 and DUOX2 is as high as 83%. In contrast to most isoforms of the enzyme family, they produce hydrogen peroxide rather than superoxide. However, they are also structurally different from NOX1-5. DUOX enzymes were initially identified as THOX1 (Thyroid oxidase 1) and THOX2 (Thyroid oxidase 2) in the thyroid gland (24, 25). Prior to their discovery, scientists have long been searching for an enzyme that is calcium- and NADPH-dependent, functions as an oxidase, and produces H_2O_2 in the epithelial cells of thyroid follicles. In 2001, Edens *et al*. proposed the name DUOX (Dual oxidase) for the enzymes based on the structural features of the protein. The N-terminal of the proteins contains an extracellular peroxidase-homology domain, distinguishing them from the NOX enzymes. As I have focused on the role of DUOX in squamous cells during my Ph.D. studies, I will provide a more detailed presentation of these two enzymes.

1.2 Characterisation of DUOX

1.2.1 Structural features of DUOX and regulation of catalytic activity

DUOX1 and *DUOX2* are located on human chromosome 15 (15q15.3), and both genes are arranged in a head-to-head configuration, separated by a 16 kb region (26). The *DUOX1* gene is 36 kb containing 35 exons, and encodes a 1551-amino-acid-long protein. In comparison, the *DUOX2* is 22 kb and contains 34 exons. The protein is composed of 1548 amino acids (27). DUOX1/2 differs from other NADPH oxidases as they contain a peroxidase-homology domain at the N-terminal. Although peroxidases are heme-binding proteins, the peroxidase-homology domain in DUOX1/2 cannot bind heme due to the absence of amino acid residues that are crucial for heme binding. Instead, it contains cation binding sites (CBS) (28, 29). The role of the extracellular peroxidase-homology domain is not yet fully understood. Site-directed mutagenesis of residues within the CBS has prevented DUOX1 from binding to maturation factor DUOXA1, which is crucial for proper function. This finding suggests a role for PHD in protein stability (29). Furthermore, it might contribute to the conversion of superoxide to hydrogen peroxide by delaying diffusion from the TM domain oxygen-reducing center (6). The pleckstrin homology-like domain (PHLD) is located on the first intracellular loop after the additional TM region, which is not present in other NOX isoforms (29). Two EF-hand type calcium-binding domains follow the PHLD domain. Mutation in this region abolished the calcium activation of enzymes (30). As mentioned above, the DH domain following the six transmembrane helices is responsible for binding FAD and NAPDH. Recent studies have investigated the structure of DUOX1-DUOXA1 and indicated that interactions between intracellular domains regulate the catalytic activity of DUOX1. They suggest that the protein can switch conformation through dimerization or calcium binding, which determines the electron transport efficiency (28, 29).

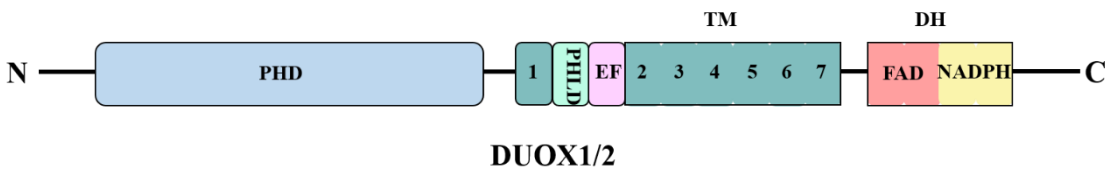

Figure 2. Domain structure of DUOX1/2. *DUOX enzymes contain extracellular peroxidase homology domain (PHD) followed by a unique transmembrane (TM) helix (0)*

and Pleckstrin homology-like domain (PHLD), as well as two EF-hand domains. N-terminal dehydrogenase (DH) domain is located intracellularly and comprises FAD- and NADPH-binding sites. The figure is based on Figure 1. of (6).

The characterization of the function and regulation of DUOX was hampered by the fact that heterologously expressed DUOX was not properly glycosylated and remained in the endoplasmic reticulum. However, identifying DUOX activator 1 (DUOXA1) and DUOX activator 2 (DUOXA2), essential proteins for the maturation and activation of DUOX1/2, led to a breakthrough. The *DUOXA* genes are localized adjacent to the corresponding *DUOX* on chromosome 15 in a head-to-head configuration. Furthermore, they are expressed with their respective *DUOX* in the same tissues (31). DUOX1/2 are localized in the endoplasmic reticulum in an inactive state. The maturation factor forms a stable heterodimer with the enzyme. This complex formation is essential for ER-Golgi transition, posttranslational modifications, and translocation to the plasma membrane. Four splice variants of DUOXA1 have been described. Two out of four, DUOXA1α (isoform 3) and γ (isoform 1) support DUOX1 maturation. However, the DUOX1/DUOXA1γ complex also accumulates in a vesicular compartment. Morand *et al.* also showed that DUOX1/DUOXA1α and DUOX2/DUOXA2 pairs produce the highest amount of hydrogen peroxide. Cross-functioning complexes are unstable and produce less H_2O_2; superoxide production has also been detected in these cases (32).
The regulatory role of phosphorylation in DUOX activity was also observed, but two different signaling pathways were found for the two enzymes. Specifically, DUOX1 activity was stimulated through protein kinase A-mediated phosphorylation on serine 955, while DUOX2 phosphorylation is induced via protein kinase C activation associated with high H_2O_2 generation in response to phorbol 12-myristate 13-acetate (PMA) (30).

1.2.2 Function of DUOX

1.2.2.1 Thyroid hormone biosynthesis

The synthesis of the thyroid hormones 3,5,3',5'-tetraiodothyronine or thyroxine (T4), and 3,5,3'-triiodothyronine (T3) occurs in the thyroid follicles. The iodide required for hormone synthesis is taken up from the blood via the sodium/iodide symporter (NIS) on the basolateral side of the thyroid cells and transported to the lumen of the follicle via the pendrin or the calcium-activated chloride channel, anoctamin-1. Thyroid peroxidase

(TPO) catalyzes the binding to tyrosine residues of thyroglobulin (TG) through iodide oxidation in the presence of DUOX-produced H_2O_2 at the apical plasma membrane of thyrocytes. When iodine is present in sufficient amounts, the synthesis of thyroid hormones is limited by the generation of hydrogen peroxide. Following endocytosis, thyroid hormones are released from iodinated thyroglobulin by proteolytic cleavage and secreted into the bloodstream via dedicated transporters such as monocarboxylate transporter 8 (MCT8) (33). DUOX2 is a crucial enzyme for the synthesis of thyroid hormones. Mutations in *DUOX2* and *DUOXA2* have been identified in both permanent and transient forms of congenital hypothyroidism (CH), a commonly inherited endocrine disorder. In contrast, the function of DUOX1 in thyroid gland function is not yet fully understood since DUOX1 knockout mice do not have hypothyroidism (14). Nevertheless, Liu *et al.* reported heterozygous *DUOX1* and *DUOXA1* missense mutations in two patients with transient and permanent forms of CH, respectively (34). It is possible that DUOX1 plays a compensatory role in the absence of DUOX2, given that mutations in both genes have been linked with a more severe hypothyroid phenotype in humans (35). Interestingly, a mutation in the *DUOX2* has been detected not only in humans but also in giant pandas (*Ailuropoda melanoleuca*), who have bamboo as a significant part of their diet despite its low nutritional value and their short, carnivorous digestive tract. Researchers have observed a significantly lower daily energy expenditure in captive and wild giant pandas than in mammals of similar size. Pandas are able to maintain their low energy expenditure due to their smaller-sized vital organs and decreased levels of physical activity. In addition, unusually low levels of thyroid hormones (T3, T4) were measured in these animals, likely linked to a point mutation in the *DUOX2* gene. This mutation, which is common among giant pandas, may account for the lower hormone levels and enable the animal to adapt to a bamboo-based diet (36).

1.2.2.2 Role of DUOX in host defense

1.2.2.2.1 Modulation of DUOX expression by immune cytokines

Th2 cytokines IL-4 and IL-13 induced *DUOX1* expression in human primary tracheobronchial epithelial cells. Similarly, treatment with the Th1 cytokine IFN-γ led to elevated expression of *DUOX2*. Importantly, these cytokine treatments not only induced the expression of the enzymes but also resulted in increased production of H_2O_2 by the

cells. Furthermore, *DUOX2* expression was also upregulated by polyinosine-polycytidylic acid, a Toll-like receptor 3 (TLR) ligand. The findings imply that the production of ROS in the respiratory tract as a component of the host defense response can be controlled by Th1 and Th2 cytokines. (37). IL-4 and IL-13 have also been observed to induce *DUOX1* in keratinocytes (38). In addition, the effect of IFN-γ on *DUOX2* has also been described in a pancreatic cancer cell line (39). It is important to note that the cytokine-dependent *DUOX* expression profile can be altered depending on the cell line. For instance, Th2 cytokines are responsible for the selective induction of *DUOX2* in intestinal and primocultured human thyroid cells. On the other hand, in colon adenocarcinoma cells, *DUOX2* expression increased upon TNF-α stimulation. Additionally, Sendai virus infection-mediated autocrine TNF-α, and IFN-β secretion led to *DUOX2* and *DUOXA2* induction in human airway epithelial cells (5).

1.2.2.2.2 DUOX-LPO system

Geiszt *et al.* were the first to suggest the model of DUOX- lactoperoxidase (LPO) system (40). LPO is a glycoprotein with antimicrobial activity in milk, tears, saliva, and airway secretions. Lactoperoxidase oxidizes thiocyanate (SCN^-) to microbicidal hypothiocyanate ($OSCN^-$) in the presence of H_2O_2 (41, 42). Using Northern blot and *in situ* hybridization, DUOX2 was identified in epithelial cells of salivary ducts and rectal glands, while DUOX1 was observed in tracheal and bronchial epithelial cells. They also tested whether DUOX1 is indeed the source of H_2O_2 in primary normal human bronchial epithelial cells. Ionomycin-generated calcium signal activated H_2O_2 production of the enzyme, which was significantly reduced after *DUOX1*-targeting anti-sense oligonucleotide treatment of the cells. The co-expression of LPO and DUOX enzymes in salivary glands, rectum, trachea, and bronchi suggest that DUOX1 and DUOX2 are sources of H_2O_2 that may support LPO-mediated antimicrobial defense mechanisms at the mucosal surface (40).

The presence of DUOX enzymes in the airways has also been investigated in various other studies. It has been observed that in fetal lung specimens, DUOX protein is undetectable until 27 weeks of gestational age. However, it is strongly upregulated after 32 weeks. *In vitro* experiments with human fetal lung cells have also revealed that DUOX1 is significantly increased during cell differentiation (43). Studies have found that alongside the presence of DUOX1, DUOX2 is also expressed in human tracheal epithelial cells (44) and human airway epithelia redifferentiated at the air-liquid interface (45).

Numerous studies have explored the antimicrobial properties of DUOX-LPO in various species and experimental conditions. Sarr *et al.* have published a comprehensive review of these findings (46). *In vitro*, cell-free models are often used, where DUOX enzymes are absent, and H_2O_2 is added either in bolus manner or produced as a by-product of an enzymatic reaction catalyzed by glucose oxidase. LPO can utilize halides such as I^-, Br^-, and F^- in addition to pseudohalide SCN^- as a substrate. However, which substrate of lactoperoxidase has the most effective antibacterial activity depends on the bacterium. For instance, LPO-mediated killing of *Actinobacillus actinomycetemcomitans* is more efficient when peroxidase catalyzes the oxidation of I^-, whereas against *Bacillus cereus*, SCN^- proves to be a more efficient substrate (46).

Several studies have investigated the LPO-dependent killing of *Pseudomonas aeruginosa*, an opportunistic pathogen of human airways that commonly infects immunocompromised individuals (46). Rada *et al.* demonstrated that *P. aeruginosa* activates DUOX1 in bronchial epithelial cells. The stimulation requires the presence of live bacteria and extracellular calcium. Additionally, this complex process involves several bacterial surface virulence factors, such as flagellum and LPS (47). Pyocyanin, secreted virulence factor of *Pseudomonas aeruginosa*, was reported to hinder DUOX activity in human airway cells. Pyocyanin, a zwitterion, can easily penetrate airway cells and utilize NADPH to produce superoxide, thereby inhibiting DUOX. Additionally, long-term exposure to pyocyanin has been shown to suppress the induction of DUOX1 by Th2 cytokines (IL-4 and IL-13) in human airway cells. However, when LPO and hydrogen peroxide were present together, pyocyanin was oxidized to less harmful species in a dose-dependent manner (48).

It is important to note that the DUOX-LPO system displays antimicrobial activity not only against bacteria but also against viruses. Influenza A virus-induced (IAV) DUOX2-produced ROS triggers the expression of pattern recognition receptors (PRRs), which are known to recognize double-stranded RNA viruses in the respiratory epithelium. Knockdown of *Duox2* in mouse nasal mucosa aggravated IAV infection (49). The role of DUOX1 in IAV-infected mice was also investigated. In *Duox1* knockout animals, increased mortality, morbidity, and impaired lung viral clearance were observed (50).

A recent study has shed light on the potential involvement of DUOX in fungal infections. Coccidioidomycosis, caused by the fungi *Coccidioides immitis* and *C. posadasii*, is

prevalent in the southwestern United States, Mexico, and Central and South America. Inhalation of arthroconidia leads to illness in about 30% of infected people, typically in the form of pneumonia, while less than 1% develop disseminated coccidioidomycosis (DCM), which affects the meninges, bones, skin, and joints. Whole genome sequencing of DCM patients found heterozygous DUOX1 or DUOXA1 variants. *In vitro* testing of these variants revealed impaired hydrogen peroxide production of the enzyme. The study also demonstrated that DECTIN-1, a C-type lectin pattern recognition receptor for the fungal cell-wall component β-glucan, induces DUOX1 activity. These findings suggest the possible role of H_2O_2 produced by DUOX1 in the defense against fungal infections (51).

1.2.2.2.3 DUOX in the gastrointestinal tract

The fundamental importance of DUOX in *Drosophila* gut immunity has been well established. *Drosophila* dual oxidase (dDuox) is essential for gut antimicrobial activities. Even minor infection through consumption of contaminated food led to a significant increase in mortality rates in adult flies, in which *dDuox* expression was silenced. However, specific restoration of *dDuox* successfully reversed this effect, highlighting the unique oxidative burst generated by this oxidase in the epithelium (52).

In mice, *Duox2* expression is localized in the tip of epithelium of ileum and colon. Sommer *et al.* conducted a study that compared the ileum and colon samples of conventionally raised and germ-free mice and found that gut microbiota induced the expression of *Duox2*. The induction of *Duox2* expression in the ileum was facilitated by NF-κB p50/p65 signaling through TRIF, whereas in the colon, MyD88 and p38 MAPK mediated its induction (53). Furthermore, infection with *Helicobacter felis* caused the upregulation of *Duox2* and *Duoxa2* expression in the stomachs of mice. Studies of DUOXA1 and DUOXA2-deficient mice (animals were supplemented with L-thyroxine) revealed that the DUOX enzyme complex plays a crucial role in preventing gastric colonization by *H. felis* and the subsequent inflammatory response (54).

Increased DUOX2 expression has been found in patients with Crohn's disease and response to *Helicobacter pylori* infections (55-58).

Exome sequencing of 59 very early-onset inflammatory bowel disease (VEOIBD) patients by Hayes *et al.* revealed two novel *DUOX2* variants associated with pancolitis without congenital hypothyroidism. One patient required colonic resection due to severe

disease, while the other had early-onset ulcerative colitis. Further analysis of *DUOX2* variants in H661 epithelial-like cells showed that both produced significantly less H_2O_2 than wild-type DUOX2, although protein expression and cellular localization were not altered. In addition, cells expressing these mutants were more susceptible to *Campylobacter jejuni* invasion (11). The first patient with VEOIBD who inherited biallelic DUOX2 inactivating mutations was identified by Parlato *et al.*. The parents were carriers of two additional variants of *DUOX2* but had no symptoms. The patient's biopsy results showed considerably lower levels of *DUOX2* expression than in healthy individuals and unrelated disease controls. Functional studies in cells indicated that DUOX2 failed to exit the endoplasmic reticulum or Golgi, likely due to impaired dimerization with DUOXA2. This led to a significant reduction in the production of H_2O_2 (59). In summary, these studies suggest a protective role for epithelial DUOX2 in the gastrointestinal tract.

1.2.2.2.4 Implication of DUOX in wound healing

The role of DUOX1 in the tracheobronchial epithelium was reported as a participant in the airway epithelial repair process. Stimulating the enzyme through ATP during epithelial injury is critical to activating extracellular signal-regulated kinases (ERK1/2) and matrix metalloproteinase-9 (MMP-9), which mediate epithelial cell migration and repair (60). A low concentration of *Pseudomonas aeruginosa* lipopolysaccharide (LPS) accelerates wound repair in human airway epithelial cells through activation of DUOX1. This study suggested that LPS is bound by Toll-like receptor 4 (TLR4) and indirectly activates the NADPH oxidase, which ultimately leads to the phosphorylation of epidermal growth factor receptor (EGFR) and wound healing (61). The role of DUOX1 and EGFR in wound healing was also reported in an *in vivo* experiment. Oropharyngeal delivery of *Duox1* silencing RNA delayed airway reepithelialization in mice after naphthalene-induced airway epithelial injury, which was associated with a suppressed activation of EGFR and signal transducer and activator of transcription–3 (STAT3) (62). The function of DUOX in wound healing in zebrafish was investigated in several studies. Niethammer *et al.* used hydrogen peroxide-specific biosensor HyPer to show that wounding induces H_2O_2 production by DUOX, and this tissue-scale gradient of ROS is required for leukocyte recruitment to the wound (63). Furthermore, it has been observed that the presence of DUOX is required for the regeneration of sensory axons following the

amputation of caudal fins in zebrafish larvae (64). Src family kinase Lyn was identified as a redox sensor that mediates initial leukocyte recruitment after wounding in zebrafish. Oxidation of single cysteine residue, C466 of Lyn by DUOX-produced H_2O_2 leads to activation of the protein (65). The role of DUOX in wound healing was also investigated in *Drosophila* embryo and *Xenopus (5)*, but there is limited data on its role in mammalian wound healing *in vivo*. Our workgroup has also observed *Duox1* knockout animals following the wounding of back skin, but we did not observe any significant differences compared to the wild-type mice in wound healing (not published).

1.2.2.3 DUOX1-derived H_2O_2 production in urothelial cells

Urothelial cells produce H_2O_2 in response to calcium signals through DUOX1, according to research by Donkó *et al.* (66). Urothelial cells were stimulated with Thapsigargin (TG) and the production of hydrogen peroxide was measured. The H_2O_2 output was 2.69 ± 0.19 nmol/10^6 cells/h, which is significantly lower than the ROS output of activated neutrophils, which is 100-120 nmol/10^6 cells/h (67). However, it corresponded with hydrogen peroxide production of histamine-stimulated immortalized bronchial epithelial cells (68). Specific activation of TRPV4 calcium channels by GSK 1016790A induced calcium signal and enhanced H_2O_2 production in urothelial cells. In response to thapsigargin and ATP, the calcium signal was measured in urothelial cells prepared from wild-type and *Duox1* knockout animals. It was found that ROS produced by DUOX1 did not affect the calcium signal of urothelial cells. No positive feedback mechanism was present between H_2O_2 and intracellular calcium levels, unlike previously observed in Jurkat cells (69). The potential antimicrobial role of DUOX1 was also investigated, but no difference was found between wild-type and DUOX1-deficient animals after bladder infection with *E. coli*. *In vivo* cystometry was used to investigate bladder function. Voiding contractions developed at similar filling volumes, but the frequency of voiding contractions in DUOX1-deficient mice was significantly higher than in wild-type animals. However, the amplitude of pressure waves was similar in both groups, and non-void contractions showed no significant difference. These results suggested that the mechanosensing of urothelial cells is associated with calcium-induced DUOX1-dependent H_2O_2 production (66).

1.2.2.4 Role of DUOX1 in keratinocytes

Hirakawa *et al.* observed that Th2 cytokines (IL-4/IL-13) induced DUOX1 expression in normal human epidermal keratinocytes. They also detected increased hydrogen peroxide production following cytokines treatment, which was DUOX1-dependent. Furthermore, IL-4/IL-13-induced DUOX1 expression enhanced phosphorylation of signal transducer and transcriptional activator 6 (STAT6) through oxidation of the catalytic cysteine 215 of protein tyrosine phosphatase 1B (PTP1B). The oxidation of PTP1B leads to inactivation of the phosphatase. These results revealed a novel role of IL-4/IL-13–induced DUOX1 in modulation of STAT6 activity (38).

The level of extracellular calcium ions in the epidermis is crucial in epidermal differentiation (70). Choi *et al.* detected increased DUOX1 expression in normal human keratinocytes upon exposure to 1.2 mM Ca^{2+} for 24 hours (71). Furthermore, knockdown of *DUOX1* with siRNA downregulated the expression of genes essential for the permeability barrier, such as filaggrin, loricrin, KRT1, KRT5, and KRT10, respectively TGM3, TGM5, DSC1, DSG1, and SERPINB. They also investigated the impact of DUOX1 expression on cornified envelope (CE) assembly. The cornified envelope replaces the plasma membrane of differentiating keratinocytes and consists of keratins. Its primary function is to create a protective barrier against the environment (72). Interestingly, they found that CE assembly was significantly reduced by DUOX1 siRNA compared to control siRNA. This study suggested that DUOX1 is involved in keratinocyte differentiation and maintaining epithelial integrity.

It is important to note that in *C. elegans*, the role of DUOX (Ce-DUOX1) in maintaining the exoskeleton, the cuticle has been previously described. Ce-DUOX1 is expressed in the hypodermal cells beneath the cuticle of larval animals. To stabilize cuticular extracellular matrix, Ce-DUOX catalyzes the cross-linking of tyrosine residues of collagen and other proteins. Ce-DUOX-deficient nematodes display various cuticle abnormalities, including large blisters, "dumpy"-like phenotypes, and translucency, as well as impaired movement (73).

Our workgroup demonstrated that in spontaneously immortalized human keratinocytes, HaCaT cells, the amount of peroxiredoxin (Prx) I and II dimers increased in response to thapsigargin treatment in a DUOX1-dependent manner. In addition, thapsigargin, ATPγS, and EGF enhanced the oxidation of thioredoxin in the presence of DUOX1. When small

interfering RNA silenced *DUOX1*, this effect of the stimuli was abolished (74). Prx I and II belong to the typical 2-Cys Prx isoforms. Their localization is dependent on the cell type and environment, but Prx I and II are mainly cytosolic. These antioxidant enzymes, known as peroxide and peroxynitrite scavenging enzymes, play a crucial role in regulating peroxide levels within cells. The typical 2-Cys peroxiredoxins comprise an active site cysteine that is sensitive to oxidation by H_2O_2. Peroxidatic cysteine thiolate (C_PS^-) of typical 2-Cys Prxs is oxidized to a sulfenic acid (C_P-SOH), followed by condensation with the resolving cysteine (C_R) of another subunit to form a head-to-tail disulfide-linked homodimer. The thioredoxin-thioredoxin reductase (Trx-TrxR) system can reduce it back to monomer. C_P-SOH of 2-Cys Prxs can react with a second H_2O_2 molecule and become hyperoxidized to cysteine sulfinic acid (C_P-SO_2H). The sulfinic acid can be reduced in an ATP-dependent reaction catalyzed by sulfiredoxin (Srx) (Figure 3.) (75, 76). To summarise our findings above, hydrogen peroxide produced by DUOX1 oxidized Prx I and II. Reduction of cross-linked Prxs oxidized Trx, which our workgroup could also detect. These findings suggest that DUOX1-produced H_2O_2 has a signaling role in keratinocytes (74).

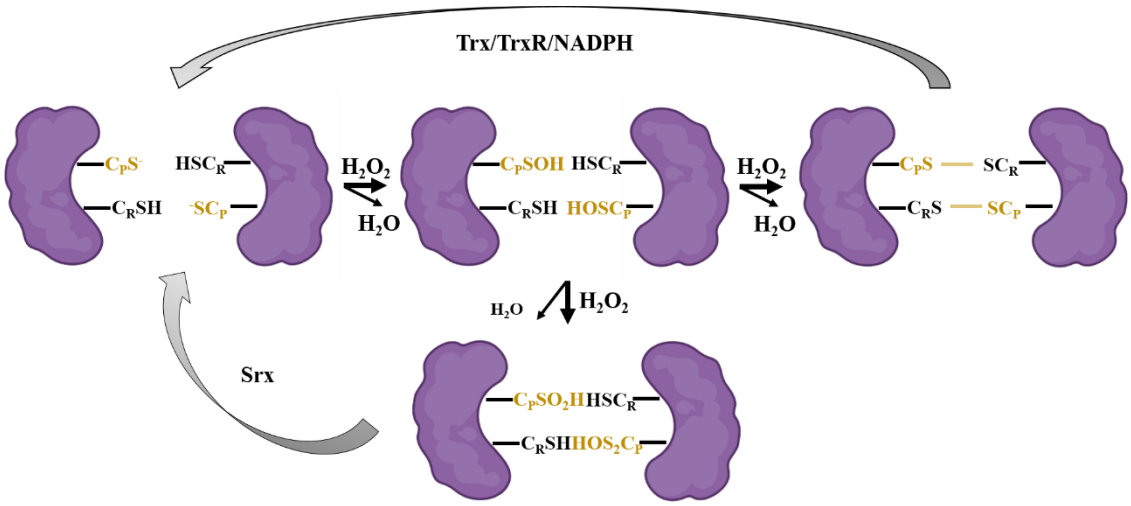

Figure 3. Schematic representation of catalytic cycle of 2-Cys. *Peroxidatic cysteine thiolate (C_PS^-) of typical 2-Cys Prxs is oxidized to a sulfenic acid (C_P-SOH), followed by condensation with the resolving cysteine (C_R) of another subunit to form a head-to-tail disulfide-linked homodimer. The thioredoxin-thioredoxin reductase (Trx-TrxR) system can reduce it back to monomer. C_P-SOH of 2-Cys Prxs can react with a second H_2O_2 molecule and become hyperoxidised to cysteine sulfinic acid (C_P-SO_2H). The sulfinic acid*

can be reduced in an ATP-dependent reaction catalyzed by sulfiredoxin (Srx). The figure is based on Figure 1. of (75).

The DUOX enzymes have also been observed in other cells, but during my Ph.D. studies, I investigated the role of DUOX1 in epithelial cells, so I tried to focus on these literature findings. Regarding my work, I will briefly touch upon the function of keratinocytes in nociception in the following paragraph.

1.3 Role of keratinocytes in nociception

The skin is the body's largest organ, encompassing the entire external surface. It is composed of three layers: the epidermis, dermis, and hypodermis. The epidermis, which is the outermost layer, consists of a stratified squamous epithelium primarily made up of keratinocytes. The epidermis has five layers: the stratum basale, stratum spinosum, stratum granulosum, stratum lucidum, and stratum corneum. Keratinocytes, which originate in the basal layer, produce keratin and form a well-organized stratified epithelium through a coordinated program of differentiation and apical migration. It has been conventionally believed that keratinocytes are solely responsible for the physical and chemical barrier functions of the epidermis.

Somatosensory neurons, with cell bodies located in the trigeminal or dorsal root ganglia (DRG), innervate the skin. Aβ-fibers, such as those innervating Merkel cells and fibers around the hair shaft, are considered touch receptors. Aδ-fibers and C-fibers include thermoreceptors and nociceptors. In pain transmission, Aδ-fibers carry the rapid and accurately localized component of the message, whereas C-fibers transmit the slow and imprecisely localized component. C-fibers are subdivided into peptidergic and non-peptidergic C-fibers. Peptidergic C-fibers primarily terminate in the spinosus layer of the epidermis, while non-peptidergic C-fibers terminate more superficially in the granular layer.

According to the classical point of view, Aδ-fibers and C-fibers extremities, that pass between keratinocytes and are called intra-epidermal free nerve endings (FNEs), are the exclusive detectors and transducers of noxious thermal, mechanical, or chemical stimuli. However, in the last two decades, the classical theory seems to have been overturned, and several studies have shown that keratinocytes are more than just a barrier, they can modulate and directly initiate nociceptive responses (77, 78).

Firstly, not only do intraepidermal free nerve endings terminate in the epidermis, but they are entirely enwrapped by keratinocyte cytoplasm and form *en passant* synaptic-like contacts with keratinocytes (79).

Beyond the anatomical proximity of the free nerve endings, several sensory and neurotransmitter receptors are expressed on keratinocytes, such as transient receptor potential proteins, voltage-gated cation channels, γ-aminobutyric acid receptors, adrenoceptors, glutamate receptors, and acetylcholine receptors (80). The forthcoming discussion will center on transient receptor potential proteins.

Transient receptor potential (TRP) proteins constitute a significant receptor family comprising non-selective ion channels permeable to Na^+, Ca^{2+}, and Mg^{2+}. These channels act as chemical, mechanical, and thermal stimuli sensors and are involved in various physiological processes such as inflammation, pruritus, nociception, and cell proliferation. TRPV1, TRPV3, TRPV4, TRPA1, and TRPM8 have been identified on human keratinocytes, inducing a Ca^{2+} influx upon activation (80).

The TRPV1 channel protein is activated by various stimuli, including high temperature (above 42 °C), capsaicin, low pH, ultraviolet irradiation, and shear stress. Although initially believed to be exclusive to sensory neurons, further studies have shown that this protein is also expressed at lower levels in other cell types, such as epidermal keratinocytes (80, 81). Additionally, Inoue *et al.* demonstrated that capsaicin triggered a rise in intracellular calcium levels in human primary keratinocytes and HaCaT, which was effectively prevented by a TRPV1 antagonist, capsazepine (82). In patients with Herpes Zoster, small fiber sensory neuropathy, diabetic peripheral neuropathy, and nerve injury, the expression of TRPV1 was found to be increased in epidermal keratinocytes. Notably, the level of TRPV1 expression was found to be correlated with the intensity of pain experienced by these patients. Furthermore, TRPV1 in keratinocytes contributes to the development of cutaneous inflammation by inducing cyclooxygenase-2 (COX-2) and the production of pro-inflammatory mediators, including prostaglandin E2 (PGE2), IL-8, IL-1β, IL-2, IL-4, and TNF-α (80).

TRPV3 is a warm temperature sensor (>33-39 °C) that is primarily expressed on keratinocytes. Studies have shown that activating TRPV3 in keratinocytes can stimulate the release of interleukin-1α, and can excite sensory neurons by releasing adenosine-5'-triphosphate (ATP) in co-culture system (83). *In vivo*, mice with localized hind paw -

1qinflammation caused by carrageenan exhibited nociceptive behavior when intraplantarly injected with farnesyl pyrophosphate, a TRPV3 agonist (84). In addition, the function of TRPV3 is crucial for establishing the skin barrier through its regulation of transglutaminase activities that are necessary for keratinocyte cornification (85). Elevated *TRPV3* expression was detected in keratinocytes of breast tissue samples collected from women experiencing breast pain and tenderness. Increased *TRPV3* expression was also found in pruritic hypertrophic burn scars, and atopic dermatitis skin. Contrastly, diabetic skin showed reduced expression of *TRPV3* (80).

Besides TRPV3, TRPV4 is also highly expressed in keratinocytes and plays a role in intercellular barrier integrity in human keratinocytes (86). TRPV4 can be activated by a specific range of temperatures (25-34 °C), as well as by extracellular hypotonicity, shear stress, or ultraviolet B radiation. The activation of TRPV4 by histaminergic pruritogens can trigger itch behaviors by stimulating the phosphorylation of MAPK and ERK in keratinocytes (80).

TRPA1 is present in various tissues, including sensory neurons and epidermis. Its function in keratinocytes is still a topic of debate. Some studies have shown that TRPA1 is activated by noxious cold (<17 °C) in human keratinocytes *in vitro*, while *Trpa1* knockout mice and rats displayed normal cold sensations. However, other studies found that *Trpa1* knockout mice showed behavioral deficits in response to cold (0 °C) and mechanical stimuli. The expression of TRPA1 is low in non-stimulated human keratinocytes, but can be upregulated through NFκB and MAPK pathways. Moreover, topical application of a TRPA1 agonist can induce the secretion of PGE2 and leukotriene B4 (LTB4) from human keratinocytes (80).

TRPM8 is located in the endoplasmic reticulum of human keratinocytes. Research conducted *in vitro* has shown that when TRPM8 is activated by mild cold temperatures ranging from 24 to 33 °C, it triggers the release of Ca^{2+} from the endoplasmic reticulum and the uptake of Ca^{2+} by the mitochondria, which modulates the synthesis of ATP and superoxide in the mitochondria. This temperature-dependent regulation of epidermal TRPM8 plays a potential role in the proliferation and differentiation of keratinocytes (80).

2. Objectives

The aim of my work was to gain a better understanding of the role of the hydrogen peroxide-producing NADPH oxidase, DUOX1 in squamous cells. Therefore, the following objectives were set:

1. to investigate the source of EGF-induced hydrogen peroxide production in squamous cells.

2. to characterize the molecular mechanism of H_2O_2 production induced by increased intracellular calcium concentration.

3. to identify the molecular targets of DUOX1-produced hydrogen peroxide.

4. to confirm the presence of DUOX1 in mouse skin.

5. to develop an antibody against mouse and human DUOX1 and establish a genetically controlled system to verify the specificity of the antibodies.

6. to investigate the selectively altered nociceptive behavior of DUOX1-deficient mice.

3. Methods

3.1 Cell culture

A431 (ATCC, Manassas, VA, USA, CRL-1555), HEK293 (ATCC, Manassas, VA, USA, CRL-1573), HEK293T (ATCC, Manassas, VA, USA, CRL-3216), HEK293A (Invitrogen R705-07) and HaCaT cells (ATCC, Manassas, VA, USA) were cultured in Dulbecco's Modified Eagle's Medium with glutamine and 4.5 g/L glucose (DMEM; Lonza Group Ltd., Basel, Switzerland) supplemented with 100 U/ml penicillin, 100 U/ml streptomycin (Lonza Group Ltd., Basel, Switzerland) and 10% fetal bovine serum (FBS; Lonza Group Ltd., Basel, Switzerland). Cells were grown in a humidified incubator with 5% CO_2 in air, at 37 °C. Primary mouse keratinocytes were prepared from the back skin of wild-type and DUOX1-deficient mice, as described previously (87).

3.2 Animals

Duox1 knockout mice described earlier by Donkó *et al.* (66) were purchased from Lexicon Pharmaceuticals, Inc. (The Woodlands, TX, USA). Briefly, *Duox1* knockout animal was created using retroviral-based gene-trap technique (Model #TF1226, Taconic, NY,USA). The location of the inserted cassette was identified by sequencing. C57BL/6N wild-type mice were obtained from commercial sources. Experimental animals were maintained on a standard diet and given water *ad libitum* in either specific pathogen-free or conventional animal facilities of Basic Medical Science Centre, Semmelweis University. Animals for nociception assays were kept in the animal house of Szentágothai Research Centre, University of Pécs, in individually-ventilated cages on wood shavings bedding, at 22±2 °C temperature and a standard 12-12 h light-dark cycle (lights on between 7:00-19:00). They were provided with standard rodent chow and water *ad libitum*. All experiments were designed and performed according to the 243/1998. Hungarian government regulation on animal experiments. Experiments were approved by the Ethics Committee on Animal Research of the University of Pécs (license number: BA02/2000-10/2011). 10-12 week old male mice of each genotype were used up to the necessary sample size. The sample size was determined based on our previous experiments using the same models (88), also considering the 3R (replace, reduce, refine) rule for the animal ethical principles. The animals were randomized into different experimental groups. The researchers were blinded to the experimental design, the

treatment the animals received, and the genotype. Due to short-term anesthesia and short observation times, the general health status of animals was not affected. The analysis included the results of all tested animals; there were no exclusions.

3.3 Mustard oil-induced thermal hyperalgesia on the tail

The noxious heat threshold of the tail of mice was measured with an increasing-temperature water bath (Experimetria Ltd., Budapest, Hungary) as previously described (88). Mice were placed into plastic restrainers, which were hung on a rack above the water bath so that the tails could be immersed into the water. The following parameters were set on the device: a starting temperature of 30 °C, a heating rate of 24 °C/min, and a cut-off temperature of 53 °C. The heating was immediately stopped when the animals showed nocifensive behavior, and the tails were removed from the water. The corresponding water temperature was recorded as the noxious heat threshold. After 3 control threshold measurements, thermal hyperalgesia was induced by immersing the tails into 5% mustard oil dissolved in 30% DMSO in water for 30 seconds. Noxious heat threshold measurements were repeated at 10 min intervals for 60 minutes after treatment. Where indicated, 3 mg/kg intraperitoneal naloxone pretreatment had been applied.

3.4 Formalin test

To evaluate formalin-induced nociception, mice were injected intraplantar with 2.5% formalin (20 µl, i.pl.) and then placed into transparent observation chambers. A mirror was placed behind the chamber so that the observer could see the animals from behind. Spontaneous nocifensive behavior was assessed between 0-5 min and 20-45 min after injection, based on the characteristic 2-phase response induced by formalin. The duration of paw licking was measured by a stopwatch while paw flinching responses were counted. A Composite Pain Score (CPS) was also calculated by the following formula: CPS=(2x paw licking time + 1x paw flinchings)/observation time. The swelling induced by formalin was determined 3 h after injection by measuring the thickness of the paw with a digital caliper (Mitutoyo, Kawasaki, Japan). The swelling was expressed as a % increase compared to the contralateral paw.

3.5 Amplex Red assay

Confluent cells on 24-well plates (SPL Life Sciences Co., Korea) were washed with H-medium (145 mM NaCl, 5 mM KCl, 1 mM $MgCl_2$, 0.8 mM $CaCl_2$, 10 mM HEPES, and

5 mM glucose, pH 7.4) and background fluorescence was also measured in 0.3 ml/well H-medium. For the assay, an H-medium-based reaction solution was used containing horse radish peroxidase (Sigma-Aldrich, Burlington, MA, USA) and Amplex Red (Synchem, Germany) in a final concentration of 0.2 U/ml and 50 µM respectively. Cells were stimulated with 1 µM thapsigargin (Sigma-Aldrich, Burlington, MA, USA), 500 ng/ml EGF (PeproTech, Rocky Hill, NJ, USA), or 100 µM vitamin B3 (Sigma-Aldrich, Burlington, MA, USA), or 10 µM ATPγS (Sigma-Aldrich, Burlington, MA, USA), or 2 nM GSK 1016790A (Sigma-Aldrich, Burlington, MA, USA). Stimuli were added to the Amplex Red-containing reaction solution immediately before pipetting onto the cells. The fluorescence measurement started promptly after adding the reaction solution, and the cells were kept at 37 °C throughout the measurement. Fluorescence of the end-product resorufin was measured at 590 nm with POLARstar Optima multimode microplate reader (BMG Labtech, Ortenberg, Germany). Background fluorescence was subtracted from the fluorescence values of each well. Each experimental condition was run in 3 parallels on the 24-well plate.

3.6 Calcium imaging

A431 and HaCaT cells were grown on coverslips. Before the experiment, cells were washed in H-medium, and Fura-2-AM (Molecular Probes, USA) was loaded in a final concentration of 1 µM for 20 minutes at room temperature. Ratiometric fluorescence intensity measurements were performed on an inverted microscope (Axio Observer D1, Zeiss) equipped with a 40x, 1.4 oil immersion objective (Fluar, Zeiss) and a Cascade II camera (Photometrics). Excitation wavelengths were set by a random access monochromator connected to a xenon arc lamp (DeltaRAM, Photon Technology International). Images were acquired every 5 s for a period of 10 to 15 min with the MetaFluor software (Molecular Devices). The final concentrations of different stimuli were 500 ng/ml EGF and 1 µM thapsigargin. 40000 HEK293 cells/well were plated on 96-well plates (SPL Life Sciences Co., Korea) pretreated with poly-L-lysine (Sigma-Aldrich, Burlington, MA, USA). HEK293 cells were transfected with human TRPA1-expressing plasmid using Lipofectamine 2000 (Invitrogen) according to the manufacturer's instructions. The plasmid was kindly provided by Zoltán Sándor, Department of Pharmacology and Pharmacotherapy, University of Pécs, Medical School. The next day cells were washed with H-medium and loaded with Fura-2-AM (2 µM

dissolved in H-medium,) for 30 min at 37 °C. Cells were rewashed, and the baseline fluorescence was measured using Clariostar (BMG Labtech, Ortenberg, Germany). Excitation wavelengths were 335 and 380 nm, and emission wavelength was 510 nm. The final concentrations of different stimuli were as follows: 500 or 100 μM H_2O_2 (Sigma-Aldrich, Burlington, MA, USA) and 10 μM AITC (Sigma-Aldrich, Burlington, MA, USA). Each experimental condition was run in 3 parallels.

3.7 siRNA transfection

Stealth siRNAs (Life Technologies) were transfected at the time of cell plating in 20 nM final concentration using Lipofectamine RNAiMAX (Invitrogen) according to the manufacturer's instructions. Measurements were carried out 48 h after transfection. Three different *DUOX1*-specific siRNA sequences were tested, and three different control siRNAs of varying GC content were used as control. All *DUOX1*-specific sequences gave efficient knockdown of *DUOX1* expression. For *DUOXA1* knockdown, one specific stealth siRNA was used.

3.8 Western blot experiments

Laemmli sample buffer was added to the cell lysate samples and these were run on 8% or 10% SDS polyacrylamide gels and blotted onto nitrocellulose membranes. Membranes were blocked in phosphate buffered saline containing 0,1% Tween- 20 and 5% dry milk or 5 % bovine serum albumin (for phospho-tyrosine specific Western blots). The first antibodies were diluted in blocking buffer and used either for 1 h at room temperature or overnight at 4 °C. After several washing steps in PBS-Tween-20 membranes were incubated with HRP-linked secondary antibodies (Amersham Pharmaceuticals, Amersham, UK) diluted in blocking buffer. After further PBS-Tween-20 washing steps, antibody binding was detected using enhanced chemiluminescence and Fuji Super RX medical X-ray films. Importantly samples were never boiled when processed for Western blotting with the DUOX1 antibody. The redox state of KCNQ4 was also measured by immunoblotting. Detection of proteins was performed using HRP-Conjugated Streptavidin (Thermo Fisher Scientific, Waltham, MA, USA) in phosphate buffered saline containing 0,1% Tween- 20 and 5% bovine serum albumin. Vinculin and actin antibodies were purchased from Sigma-Aldrich (V9131, A1978), EGFR antibodies were from Cell Signalling Technology (4267S), and DUOX antibodies were non-commercial.

3.9 Non-commercial DUOX1 antibodies

In the experiments shown in Figure 9. and 12., a rabbit polyclonal anti-DUOX antibody (kindly provided by Francoise Miot, Brussells, Belgium), which was raised against the Arg618-His1044 fragment of human DUOX1 was applied (25). Later our own polyclonal antibody had been developed against a 411-amino-acids-long sequence of recombinant human DUOX1 (amino acids 622-1032). This antigene was produced and purified from BL21 Competent Cells and injected intracutaneously with Freund's adjuvant into New Zealand white rabbits. For polyclonal antibodies, rabbits were sacrificed, and antibodies were affinity purified from the sera using Affigel 10 beads (BioRad Laboratories, Hercules, CA, USA) loaded with the antigens according to the manufacturer's instructions.

3.10 DUOX1 CRISPR in HaCaT

HaCaT cells were genetically mutated for DUOX1, using a pSpCas9(BB)−2A-GFP (PX458, Addgene) vector, following Target Sequence Cloning Protocol by ZhangLab (89). The vector contained the 5′-gagctgtctcggctgcggacagg-3′ guide sequence. The cells were transfected with Lipofectamine LTX and Plus Reagent (Invitrogen), and GFP-positive cells were sorted onto 96-well plates. Cell clones were screened by PCR of genomic DNA using 5′-gtgcagtgaggatatcccaaccc-3′ sense and 5′-ctggctcctgaccaatgctgg-3′ antisense oligos. PCR products were analyzed by Surveyor mismatch analysis, then sent for sequencing. It was confirmed by Western blot analysis and Amplex Red assay that the selected cell line does not express DUOX1.

3.11 Biotinylation of reduced thiols

HEK293T cells were transfected on poly-L-lysine (Sigma-Aldrich, Burlington, MA, USA) coated 6-well plates (SPL Life Sciences Co., Korea) with *Kcnq4* Mouse Tagged ORF Clone (OriGene, Rockville, MD, USA) using Lipofectamine LTX and Plus Reagents (Invitrogen) following the manufacturer's instructions. The next day the transfected cells were washed with H-medium and treated with 0, 20, 100, or 500 μM H_2O_2 in 2 ml H-medium for 3 minutes at 37 °C. After the treatment, cells were lysed and collected in ice-cold lysis buffer (50 mM TRIS, 140 mM NaCl, 1% Triton X-100, 0.1% SDS, 1mM PMSF, and cOmplete Mini Protease Inhibitor Cocktail (Merck, Darmstadt, Germany), pH 8) with 250 μM biotin polyethyleneoxide iodoacetamide (BIAM, Thermo

Fisher Scientific, Waltham, MA, USA). Samples were centrifuged at 15,000 RPM for 10 minutes at 4°C, and the supernatants were incubated for 25 min at 4 °C. The protein concentration of the samples was adjusted to equal amounts using Pierce BCA Assay Kit (Thermo Fisher Scientific, Waltham, MA, USA) for subsequent immunoprecipitation. 50-100 µg of protein were used to pull down FLAG-tagged KCNQ4 proteins with monoclonal anti-FLAG M2 antibody produced in mouse (mouse monoclonal Anti-FLAG M2 antibody, F3165) and Protein G Sepharose beads (Abcam, UK) at 4 °C overnight. For Western blot analysis, beads were boiled in Laemmli sample buffer.

3.12 Biotinylation of reversibly oxidized thiols

The experiment started like the biotinylation of reduced thiols, described above. After H_2O_2 treatment, biotin labeling of reversibly oxidized thiols was conducted by a modified protocol based on Löwe *et al.* (90). Briefly, free thiols were alkylated with 100 mM N-ethylmaleimide (NEM, Sigma-Aldrich, Burlington, MA, USA) in H-medium for 5 minutes at room temperature. Subsequently, cells were lysed and collected from the plate in ice-cold BASE-buffer (1% IGEPAL-CA630, 150 mM NaCl, 50 mM TRIS, 1 mM EDTA, pH 8) supplemented with 100 mM NEM and cOmplete Mini Protease Inhibitor Cocktail (Merck, Darmstadt, Germany) on ice. Samples were centrifuged at 15,000 RPM for 10 minutes at 4 °C. Excess of NEM was removed from the supernatants using 0.5 ml Zeba Spin Desalting Columns (Thermo Fisher Scientific, Waltham, MA, USA) according to the manufacturer's recommendations. Reversibly oxidized thiols were reduced with 2.3 mM dithiothreitol (DTT, Avantor, Radnor, PA, USA) for 30 minutes on ice. After removing excess DTT with desalting columns, reduced thiols were alkylated with biotin polyethyleneoxide iodoacetamide (Thermo Fisher Scientific, Waltham, MA, USA) for 2 hours on ice in ultrasound bath. After removing unbound BIAM with desalting columns, the steps of the biotinylation of reduced thiols, as described above, were followed. KCNQ4 was immunoprecipitated, and signals were detected by Western blot.

3.13 Biotinyl tyramide assay

HaCaT and HaCaT *DUOX1* knockout confluent cells on coverslips were washed with H-medium and treated with 1 µM thapsigargin in the presence or absence of 0.2 U/ml horse

radish peroxidase and 27,5 µM biotinyl tyramide (Sigma Aldrich, Burlington, MA, USA) for 5 minutes at 37 °C. After treatment, cells were washed 3 times with PBS on ice, and bound biotinyl tyramide was visualized with fluorescent streptavidin (Vector Laboratories, Inc., Burlingame, CA, USA) at 1:1000 in PBS for 30 minutes at 4 °C. Cells were fixed with ice-cold 4% paraformaldehyde solution and cell nuclei were stained with To-Pro-3 (Invitrogen). Samples were mounted with Mowiol (Sigma Aldrich, Burlington, MA, USA) and analyzed with an LSM710 confocal laser-scanning microscope using a 63x oil objective (Carl Zeiss).

3.14 Quantitative PCR

Mouse tissue RNA was isolated from dorsal root ganglions, hind paw, and tail skin using RNeasy Mini Kit (Qiagen, Hilden, Germany). Human keratinocyte RNA was purified using NucleoSpin RNA (Macherey-Nagel, Düren, Germany). Before the RNA preparation, tissue samples were collected into RNAlater reagent (Thermo Fisher Scientific, Waltham, MA, USA) at room temperature. cDNA was synthesized from 2 µg of total RNA using High-Capacity cDNA Reverse Transcription Kit (Fermentas) according to the manufacturer's recommendations. For qPCR reaction, 0.5 µl of cDNA was used in a 10 µl reaction solution using TaqMan Gene Expression Assays (Thermo Fisher Scientific, Waltham, MA, USA) and LightCycler 480 Probes Master (Roche Life Science) in a LightCycler LC480 plate reader (Roche Life Science). For each cDNA sample, the expression of the target was divided by the expression of the endogenous control. The crossing point was determined by the second derivative method. The specific Taqman Gene Expression assays utilized are described in our publications (74, 91).

3.15 Measurement of ATP secretion

HEK293A cells expressing the $GRAB_{ATP}$ sensor were kindly provided by Balázs Enyedi. $GRAB_{ATP}1.0$ expression plasmid was created by Gibson cloning based on the sequence provided in the article of Wu *et al.* (92) . $GRAB_{ATP}1.0$ was N-terminally fused through a P2A peptide with a plasma membrane-localized far-red fluorescent protein, mKate2. Membrane localization of mKate2 was achieved by fusing it to the N-terminal targeting sequence of the protein Lck (MGCVCSSNPENNNN). 35000 cells/well (30% HEK293A-70% HaCaT or 100% HEK293A) were plated on Ibidi 8-well µ-slides (Ibidi GmbH, Gräfelfing, Germany) pretreated with poly-L-lysine (Sigma-Aldrich, Burlington, MA,

USA). Next day before measurements, growth medium was replaced with imaging medium (EC1, containing 3.1 mM KCl, 133.2 mM NaCl, 0.5. mM KH_2PO_4, 0.5 mM $MgSO_4$, 5 mM Na-HEPES, 2 mM $NaHCO_3$, 1.2 mM $CaCl_2$, and 2.5 mM Glucose) Experiments were performed at room temperature on a NikonTi2 inverted microscope equipped with an Apo LWD 40x WI λS DIC N2 water immersion objective, a Yokogawa CSU-W1 Spinning Disk unit, a Photometrics Prime BSI camera and 488 nm and 561 nm diode laser lines. After recording the cells for 2 minutes, a custom-made perfusion system was opened, and fresh EC1 medium was delivered by perfusion to wash the previously produced ATP away. As treatment, 2.5 nM GSK 1016790A or 500 μM H_2O_2 were applied. At the end of the measurement, 1 μM ATP was added as a positive control.

3.16 Analysis and quantification of ATP secretion

$GRAB_{ATP}$-expressing cells were automatically segmented in the red channel (mKate2) using the software Cellpose (93). The mean intensity of the green and red channels (cpEGFP and mKate2) was recorded for each cell at each time point using the generated masks. Taking advantage of the P2A peptide linker between the mKate2 and $GRAB_{ATP}$ resulting in a 1:1 expression ratio, we used the green/red ratio as a normalized measure of the $GRAB_{ATP}$ signal. To express all intensities between 0 and 1, we applied the following further normalization: $(F-F_0)/(F_{max}-F_0)$, where F is the intensity at a given time point, F_0 is the average intensity value of the baseline measured during the 5 minutes prior to the stimulation and F_{max} is the maximum intensity value after ATP stimulation. Finally, we applied a rolling average of 3 on the normalized data. The final output data was then denoted $\Delta F/F_0$. We excluded the 2 minutes pre-perfusion baseline and the first 3 minutes of the washing step from the analysis for all experiments. Before analysis, the background intensity was removed automatically using the SMO software, and images were registered using the pystackreg software. All data were analyzed and plotted using the Python libraries Pandas, Numpy, and Seaborn. Statistical analysis was done using the t-test of the 'stats' module from the Python library Scipy.

3.17 Statistical analysis

Statistical analyses were performed using Graph Pad Prism 7.0 and Origin Pro 8 software programs. Specific statistical tests are presented in the figure legend for each experiment. *P*-values below 0.05 were considered statistically significant.

4. Results

4.1 EGF stimulates H_2O_2 production in A431 and HaCaT cells

Bae *et al.* previously described that epidermal growth factor (EGF) induces H_2O_2 production in A431 cells, but the origin of the ROS was not identified (94). We had a theory about a possible source of H_2O_2. Therefore, we wanted to reproduce this experiment. Hydrogen peroxide production by human epidermoid squamous carcinoma A431 and human spontaneously transformed epidermal keratinocyte HaCaT cells were detected through the measurement of changes in Amplex Red fluorescence. In the presence of horseradish peroxidase, the Amplex Red reagent reacts with H_2O_2 in a 1:1 stoichiometry to produce the red-fluorescent oxidation product, resorufin. Both cell lines showed measurable basal H_2O_2 production, which can be generated by other molecular processes, such as mitochondrial activity. As shown in Figure 4. A and B, compared to the non-treated control cells, both cell lines showed increased H_2O_2 production after EGF stimulation, increasing the Amplex Red fluorescence signal. The stimulated cells produced approximately 3 nmol/h/10^6 cells H_2O_2, as determined by simple linear regression analysis of Amplex Red fluorescence on an H_2O_2 concentration scale.

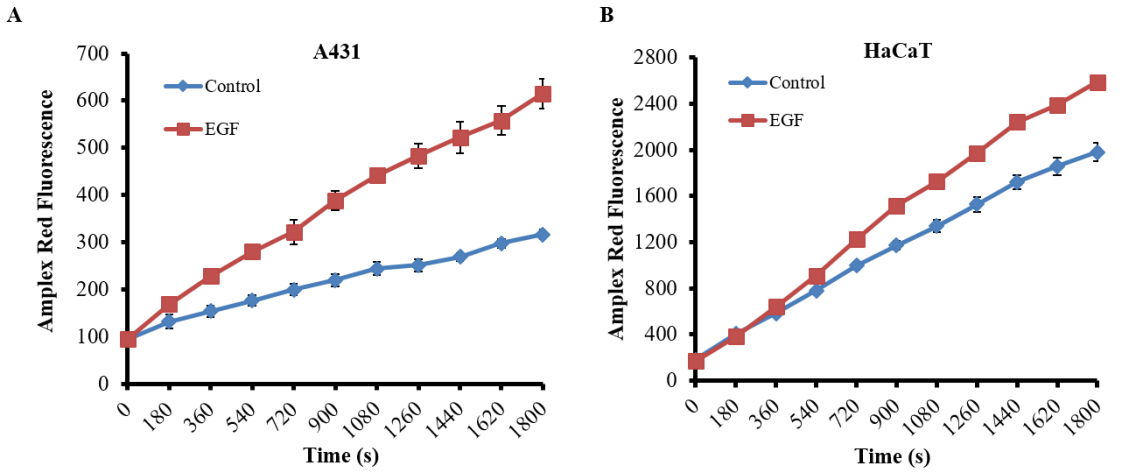

Figure 4. Detection of EGF-induced H_2O_2 production in human keratinocyte cell lines. *A431 (A) and HaCaT (B) cells were stimulated with 500 ng/ml EGF for 30 minutes, and changes in Amplex Red fluorescence were measured. Representative plots (at least 3 independent experiments) show mean ± SD of triplicate. The figure is modified from Figure 1. of (74).*

4.2 Intracellular Ca^{2+}-induced H_2O_2 production in keratinocyte cell lines

The interaction between EGF and EGFR increases intracellular calcium level by activating phospholipase Cγ (95). In our following experiments, we investigated the role of the calcium signal in EGF-induced H_2O_2 production. To confirm that intracellular calcium levels increased after EGF stimulation, we utilized Fura-2-AM - a fluorescent indicator for intracellular calcium - in the cells we examined. A431 and HaCaT were loaded by incubation with 1 μM solutions of the cell-permeant AM ester. In the cell, nonspecific esterases hydrolyzed the AM ester to liberate the FURA. Figure 5. shows that EGF increased the intracellular Ca^{2+} level in both cell lines. To elicit the maximal Ca^{2+} response, cells were treated with thapsigargin, a non-competitive inhibitor of endoplasmic reticulum Ca^{2+}-ATP-ase (SERCA). Thapsigargin depletes intracellular calcium stores and evokes Ca^{2+} influx from the extracellular space.

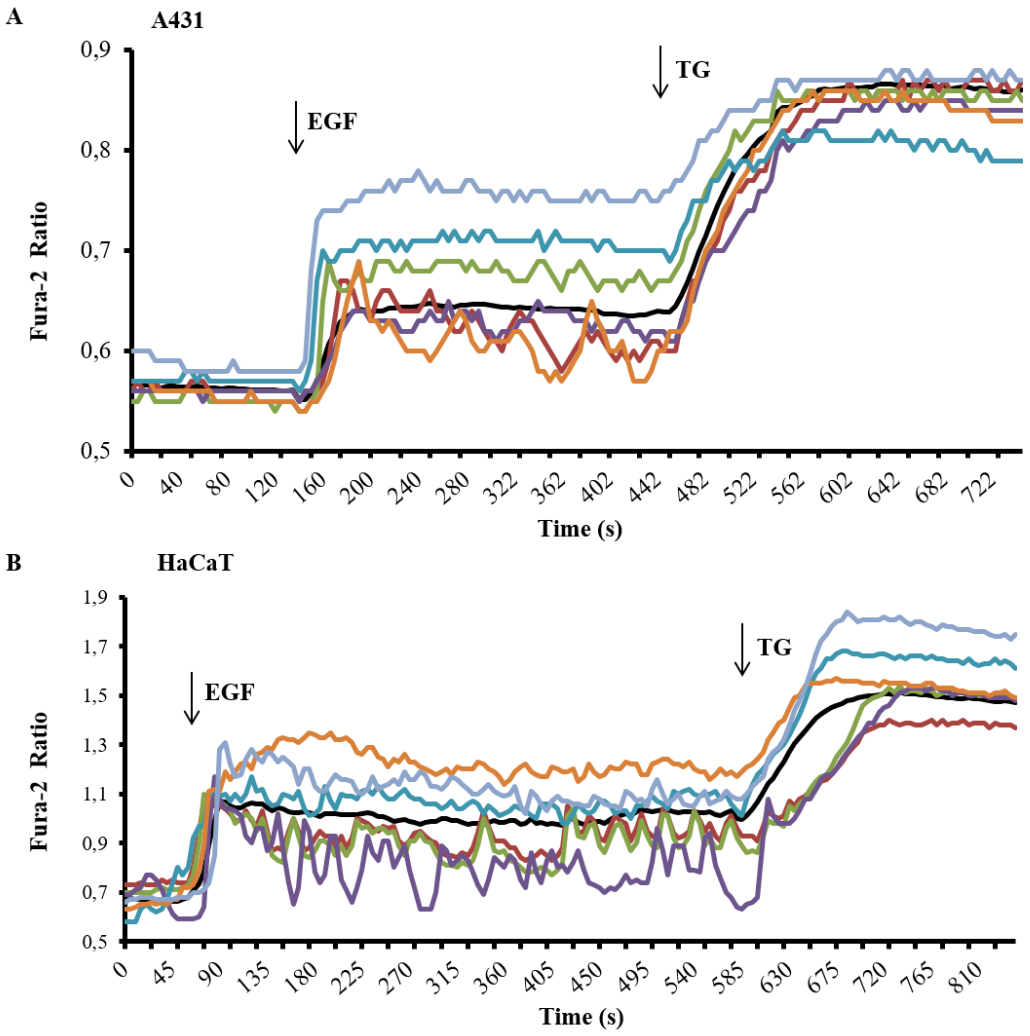

Figure 5. Detection of changes in intracellular calcium level with FURA-2-AM. *Cells were loaded with 1 μM FURA -2-AM for 20 min. (A) A431 cells were stimulated with 500 ng/ml EGF, followed by 1 μM thapsigargin. (A) HaCaT cells were also treated with 500 ng/ml EGF, then 1 μM thapsigargin was added. (B) Representative graphs (at least three independent experiments) show the results of 6 different cells from one well. The black line represents the average of the six other colored curves (74).*

Upon detecting the increase in intracellular calcium levels in both A431 and HaCaT cells after EGF stimulation, we further examined the impact of calcium on H_2O_2 production in these cells. Our findings revealed that treatment with BAPTA-AM, a calcium chelator, prior to EGF stimulation prevented the previously observed growth factor-evoked increase in H_2O_2 production (Figure 6.). These results indicate the essential role of the calcium signal in EGF-induced ROS production.

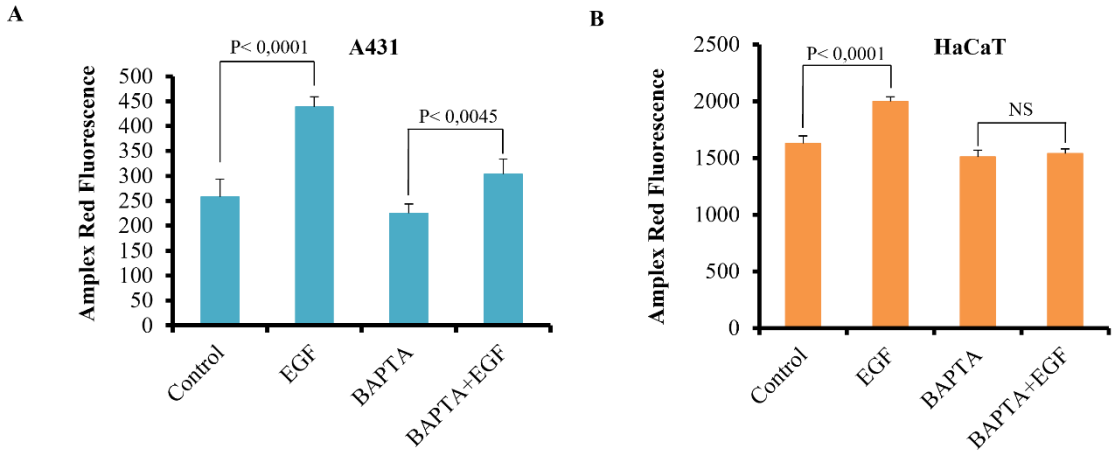

Figure 6. Role of calcium in EGF-induced production of H_2O_2 in A431 and HaCaT cells. *A431 (A) and HaCaT (B) cells were incubated for 10 min at 37 °C with 50 μM BAPTA-AM, then received 500 ng/ml EGF stimulus. After 10 min, H_2O_2 production was detected by Amplex Red assay. Unpaired t-test was used. The figure is modified from Figure 2. of (74).*

Our next experiment was based on a previously also described phenomenon that in HaCaT cells EGF, bradykinin, thapsigargin, and Ca^{2+}-ionophore A23187 induced ROS production, and this increased generation of ROS was intracellular calcium level-dependent (96). Therefore, we used diverse stimuli to elicit the intracellular calcium

signal. Meanwhile, H_2O_2 production was detected by Amplex Red reagent. In A431 cells, a relevant increase was measured compared to non-treated cells in response to the thapsigargin (Figure 7. A). HaCaT cells were also treated with several intracellular Ca^{2+} signal-inducing stimuli, which enhanced H_2O_2 production. In addition to thapsigargin, ATP analog ATPγS, vitamin B3 (also known as niacin), and TRPV4 agonist GSK 1016790A were applied. All stimuli increased H_2O_2 production, resulting in an elevation of Amplex Red fluorescence, although the degree of elevation varied among the stimuli (Figure 7. B).

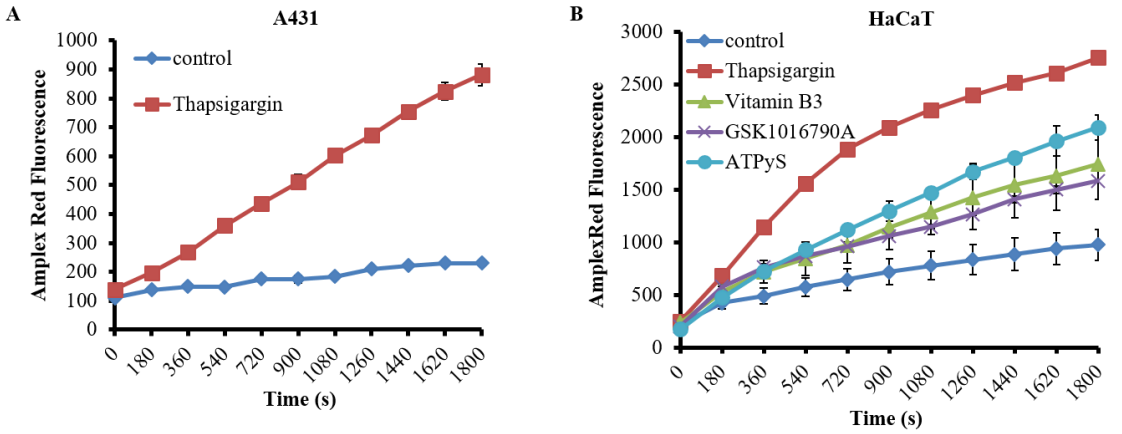

Figure 7. Measurement of Amplex Red fluorescence in A431 and HaCaT cells with distinct intracellular calcium signal-inducing stimuli. *(A) A431 cells were stimulated with 1 μM thapsigargin. (B) HaCaT cells were treated with 1 μM thapsigargin, 10 μM ATPγS, 100 μM vitamin B3, or 2 nM GSK 1016790A. Representative plots (at least 3 independent experiments) show mean ± SD of triplicate. The figure is modified from Figure 2. of (74).*

4.3 Expression of NADPH oxidases in A431 and HaCaT cells

Although H_2O_2 can be produced in cells by several processes (e.g., as a by-product by the mitochondrial respiratory chain), it is known that in mammalian cells, NADPH oxidases are the primary source of regulated H_2O_2 production (3). Therefore, we wanted to investigate the possible involvement of this enzyme family in EGF-induced production of H_2O_2. First, we used quantitative PCR to investigate the expression pattern of NADPH oxidase family components in A431 and HaCaT cells (Figure 8.). *DUOX1* was the most abundantly expressed NADPH oxidase isoform, and its maturation factor *DUOXA1* was also highly expressed. Although *CYBA* (encodes $P22^{PHOX}$) expression was also high in

HaCaT cells, it was not observed in A431 cells. Moreover, the expression level of NOX isoforms (NOX1-4), which require the co-expression of $P22^{PHOX}$, was negligible compared to *DUOX1*.

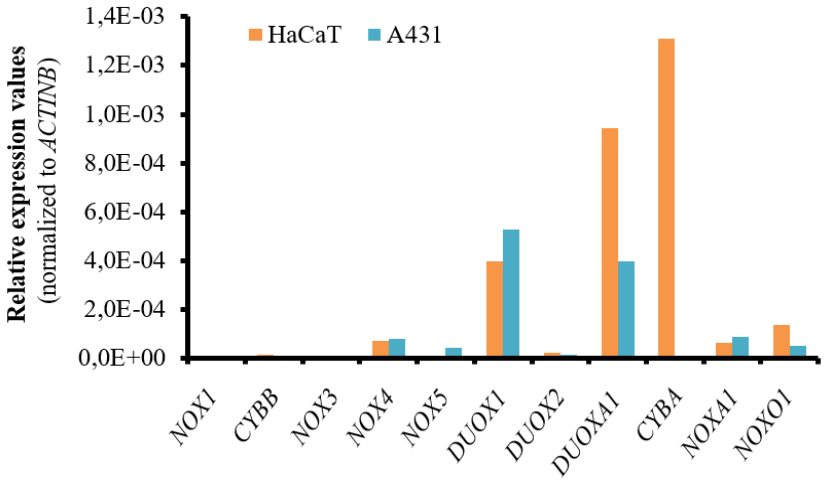

Figure 8. Quantitative PCR analysis of the expression of NADPH oxidase isoforms and their regulators in keratinocyte cell lines. *The plot is representative of three independent experiments. The figure is modified from Figure 1. of (74).*

Additional commonly used epithelial tumor cell lines (human lung epithelial adenocarcinoma cells A549, ovarian carcinoma cells A2780, and cervical cancer cells HeLa) were also examined. Still, no relevant amount of *DUOX1* expression was detected nor increased H_2O_2 production after EGF stimulus (74).

Next, we also confirmed the presence of DUOX1 at the protein level in these cells (Figure 9.). Since the antibody cannot distinguish between DUOX isoforms, we used siRNA to verify that DUOX1 was indeed detected by Western blot. Based on these results, we can conclude that among the NADPH oxidases, DUOX1 is the possible source of regulated H_2O_2 production in A431 and HaCaT cells.

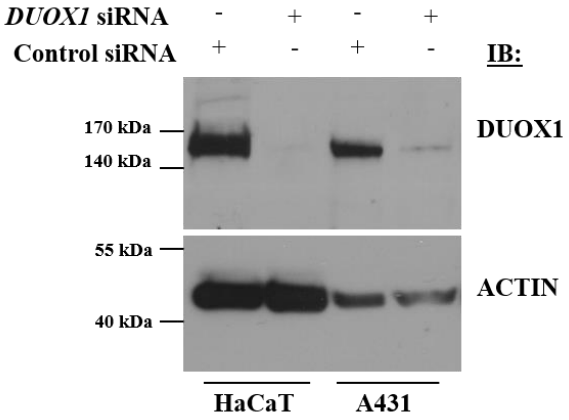

Figure 9. Western blot analysis of DUOX1 protein expression in HaCaT and A431 cells. *Epithelial cells were transfected with 20 nM scrambled or DUOX1 specific siRNA and harvested 48 h later. The Western blot was repeated more than four times from different siRNA transfections, with similar results. The figure is modified from Figure 1. of (74).*

4.4 Role of DUOX1 in intracellular Ca^{2+}-induced H_2O_2 production

As mentioned in the introduction, the intracellular calcium signal stimulates DUOX1 activity via the calcium-binding EF hand of the enzyme (27). Based on the results described above and this information, in our following experiments, we investigated the role of DUOX1 in the H_2O_2 response to intracellular Ca^{2+} level increase. Expression of *DUOX1* was effectively downregulated by *DUOX1* siRNA treatment, which reduced the basal production of H_2O_2, and there was no significant increase in ROS generation in response to either EGF or thapsigargin stimuli (Figure 10. A and C). To confirm the crucial role of DUOX1 in EGF-induced H_2O_2 production, DUOX1 maturation factor, DUOXA1 was also effectively reduced by *DUOXA1* siRNA treatment. Several publications demonstrated that the enzymatic activity of DUOX1 is dependent on the maturation factor, which assists the enzyme to be transported from the endoplasmic reticulum to the plasma membrane (31, 32). As shown earlier (Figure 8.), both cell lines express *DUOXA1*. Silencing of *DUOXA1* has a similar effect as silencing of *DUOX1* on EGF-induced H_2O_2 production (Figure 10. B and D). This result also verified the essential role of DUOX1 activity in growth factor-stimulated, increased H_2O_2 generation.

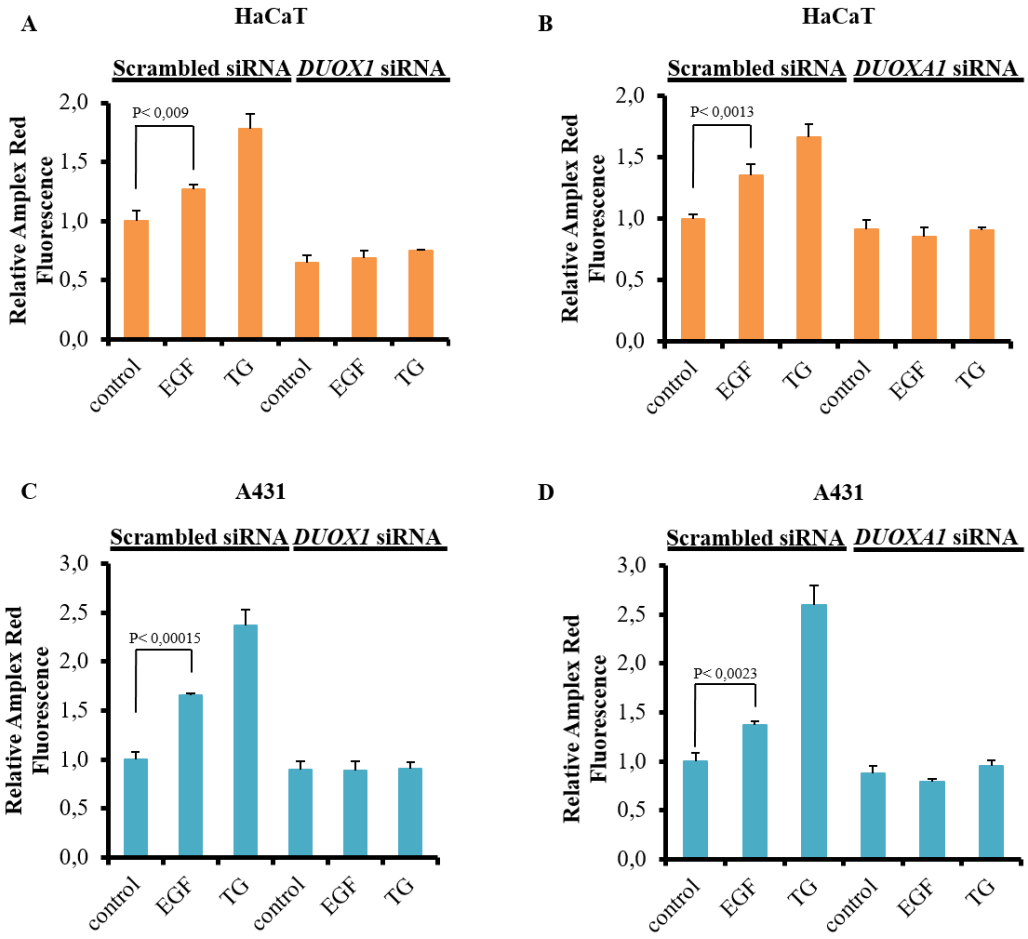

Figure 10. Measurement of Amplex Red fluorescence in DUOX1 or DUOXA1 siRNA-treated A431 and HaCaT cells. *HaCaT (A, B) and A431 (C, D) cells were transfected with scrambled, DUOX1 (A, C) or DUOXA1 (B, D) siRNA. After 48 h silencing, cells were treated with EGF or thapsigargin at 37 °C for 20 minutes. (A) Plot shows mean ± SEM of four independent experiments. (B-D) Representative plots of two independent measurement shows mean ± SD. Unpaired t-test was used. The figure is modified from Figure 3. of (74).*

DUOX1-produced H_2O_2 was published to affect intracellular calcium signaling in Jurkat cells (69). Nevertheless, our group could not observe this effect using primary urothelial cells from wild-type and *Duox1* knockout mice (66). We also wanted to investigate whether DUOX1-derived H_2O_2 modulates the intracellular calcium level in A431 or HaCaT cells. After 48 h siRNA treatment, cells were loaded with FURA-2-AM, then stimulated with EGF and thapsigargin. SiRNA-mediated downregulation of *DUOX1* did not affect the stimuli-induced increase in intracellular calcium (Figure 11.).

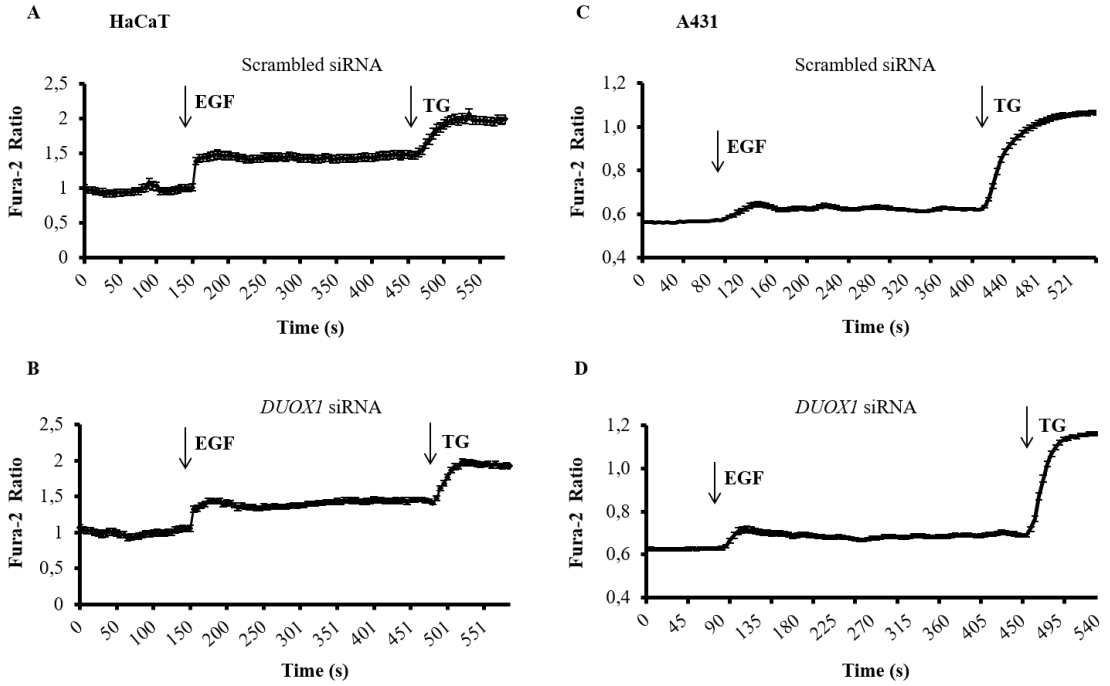

Figure 11. Analysis of EGF-and thapsigargin-induced changes in intracellular calcium level after DUOX1 siRNA treatment. *(B, D) Before the FURA-2 ratio measurements, Duox1 was silenced. (A-B) HaCaT cells, (C-D) A431 cells were treated with 500 ng/ml EGF, followed by 1 μM thapsigargin. Graphs show representative results of three independent experiments (74).*

4.5 Pattern of tyrosine phosphorylation in the absence of DUOX1 activity

A wide variety of proteins contain redox-sensitive amino acid residues, including protein tyrosine phosphatase (PTP) superfamily. The signature motif His-Cys-X-X-Gly-X-X-Arg-Ser/Thr, which defines the PTP superfamily, bears a constant cysteine residue, which is susceptible to reversible oxidation. The thiol group of Cys is oxidized to sulphenic acid, and this redox modification inhibits transiently the enzyme activity, which modulates tyrosine phosphorylation response to distinct physiological stimuli (97, 98).

Lee *et al.* published that the oxidation of cysteine residue of recombinant protein-tyrosine phosphatase 1B (PTP1B) by EGF-induced H_2O_2 production inhibits enzyme function in A431 cells (99). Based on our experimental results detailed above, we were curious to see that *DUOX1* silencing would affect the tyrosine phosphorylation pattern in response to EGF. As shown in Figure 12., although EGF induced protein phosphorylation, the lack of DUOX1 activity did not result in a visible difference in the amount of phosphorylated tyrosines.

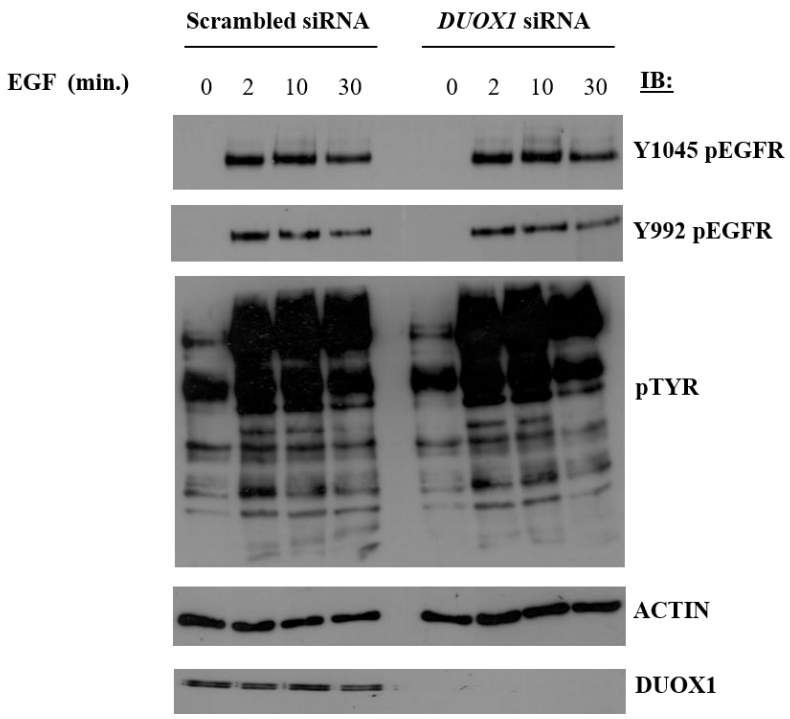

Figure 12. Western blot analysis of tyrosine phosphorylation response in DUOX1 siRNA-treated A431 cells. *Cells were transfected with scrambled or DUOX1 siRNA for 48 h. Then, 100 ng/ml EGF was added at 37 °C for 0, 2, 10, or 30 min. The membrane was blocked with a solution containing 5% BSA. The Western blot was repeated three times, with similar results (74).*

We utilized the Human Phospho-Kinase Array Kit to investigate the phosphorylation patterns of kinases and their protein substrates in both wild-type and si*DUOX1* treated cells. Our analysis focused on 43 kinase phosphorylation sites and two related total proteins. However, we did not observe any significant differences between the control and silenced samples in terms of the relative levels of phosphorylation (data not shown).

4.6 Distinct behavioral responses to nociceptive stimuli in *Duox1* knockout and wild-type mice

DUOX1-deficient mice had already been available to our group for several years prior to my employment in the laboratory. As the animal displayed no clear phenotypic difference from the wild-type, they started to study the mice in more detail, subjecting them to different tests. In collaboration with Zsuzsa Helyes' laboratory in Pécs, they were also used for various nociception experiments. I was not involved in these measurements, as I

was not yet a member of the lab, but I would like to present two important results because, during my Ph.D., part of my work was looking for an explanation of these phenomena. *Duox1* knockout and wild-type animals displayed the first significant difference in the allyl isothiocyanate (AITC) containing mustard oil-induced thermal hyperalgesia. DUOX1-deficient mice were much more sensitized to thermal stimuli than wild-types. For the experiment, an increasing temperature water bath was used and thermal hyperalgesia was evoked by immersing the tail into TRPA1 agonist allyl isothiocyanate containing mustard oil for 30 sec. AITC stimulates capsaicin-sensitive sensory nerve terminals, and they release proinflammatory neuropeptides, causing acute neurogenic inflammation and consequently increased sensitivity toward thermal stimuli (88). After the pretreatment, their tail was hung into the water bath. The bath temperature was considered a noxious heat threshold, when the mouse removed its tail. As Figure 13. A shows, in every timepoint after the pretreatment with AITC *Duox1* knockout animals thermonociceptive threshold was significantly lower than wild-types. The decrease of the thermonociceptive threshold (hyperalgesia) of the pretreated DUOX1-deficient and control mice was also significantly different (Figure 13. B). To exclude the possible role of endogenous opioid mechanisms, intraperitoneal naloxone was injected to the animals before the experiment. The opioid antagonist pretreatment did not reduce the thermal nociceptive threshold.

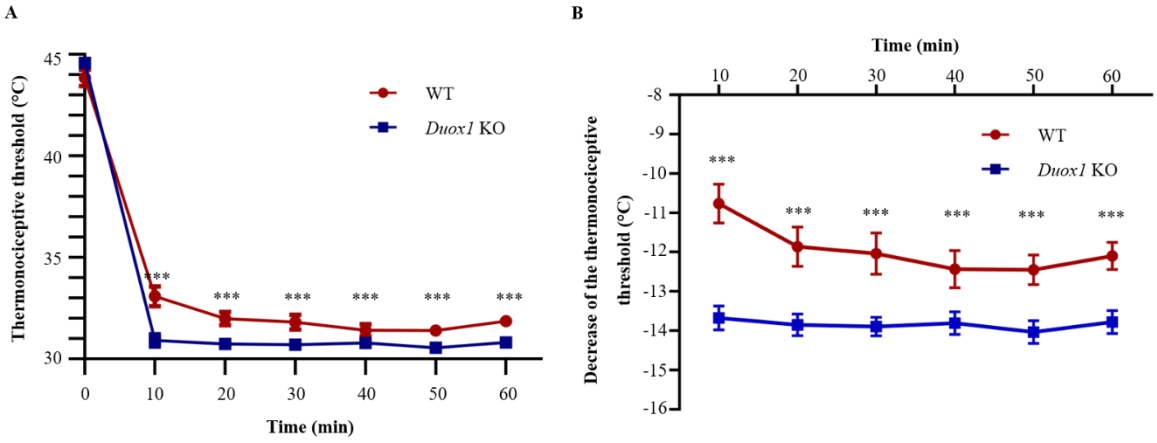

Figure 13. Allyl isothiocyanate-induced thermal hyperalgesia in wild-type and Duox1 knockout mouse. *Comparison of the tail thermonociceptive threshold and its decrease after AITC treatment in wild-type and Duox1 knockout mice. (A and B) Thermal hyperalgesia was evoked by allyl isothiocyanate-contained mustard oil for 30 sec. Mice*

*were placed into restrainers and their tail was first immersed into AITC-containing mustard oil, then into increasing temperature water bath. Noxious heat threshold measurements were repeated at 10 min intervals for 60 minutes after treatment. Plots show mean ± SEM of n=16-17 animals/group. *** p <0.001 compared with corresponding controls, by 2-way ANOVA. The figure is based on Figure 4. of (91).*

An increase in both paw lickings and paw flinches after intraplantar formalin injection was also measured, which resulted in a significantly increased composite pain score (composite pain score=(2x paw licking time + 1x paw flinchings)/observation time) in DUOX1-deficient mice (Figure 14. A-C). However, the swelling induced by formalin was not significantly different between control and *Duox1* knockout animals (Figure 14. D). The formalin-induced behavioral response also involves TRPA1 activation, as the above-detailed AITC treatment (100).

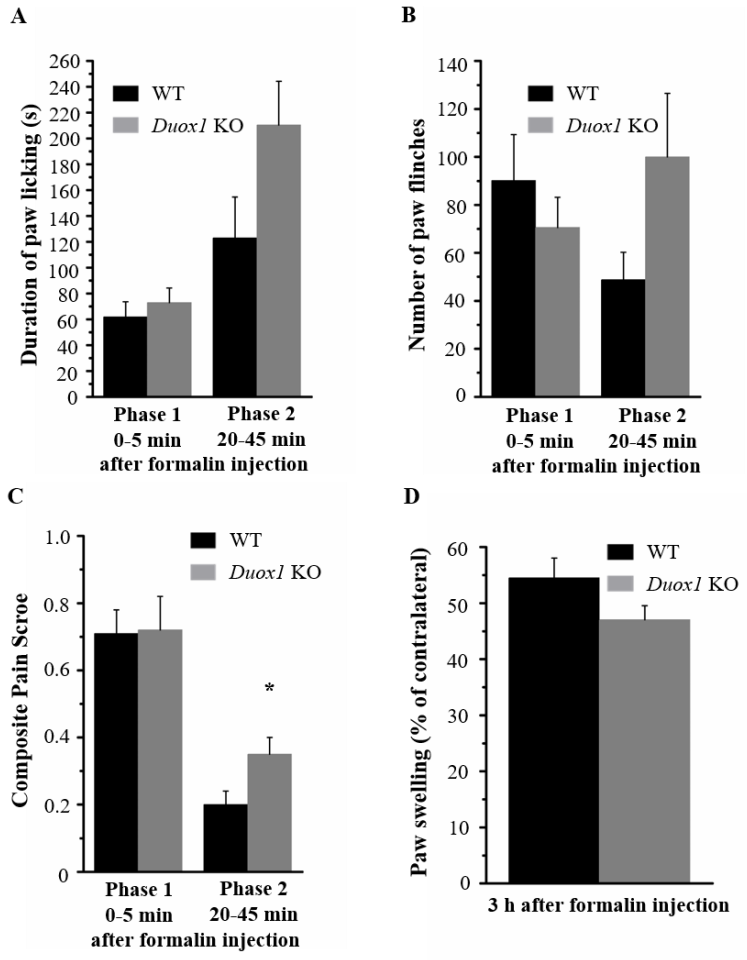

Figure 14. Formalin-evoked nociception in wild-type and Duox1 knockout animals. *After intraplantar 20 µl 2.5% formalin injection, spontaneous nocifensive behavior was*

*observed between 0-5 min and 20-45 min in wild-type and Duox1 KO mice. (A) The duration of paw licking was measured by a stopwatch. (B) Paw-flinching responses were counted. (C) Composite Pain Score (CPS) was calculated using the following formula: CPS=(2x paw licking time + 1x paw flinchings)/observation time. (D) The swelling induced by formalin was determined 3 h after injection by measuring the thickness of the paw. The swelling was expressed as a % increase compared to the contralateral paw. Data are mean ± SEM of n=5-5 animals/group. * p<0.05 compared with corresponding controls, by unpaired T-test. Except for Phase 2 CPS, no statistically significant differences were found between wild-type and Duox1 knockout animals. The figure is based on Figure 5. and Figure S4. of (91).*

Several other nociceptive studies, such as measurement of mechanical nociceptive thresholds after mechanical noxious stimuli (plantar incision), or following a short heat injury, comparison of noxious heat and mechanical nociceptive thresholds have been performed. Still, they did not show significant differences between *Duox1* knockout and wild-type animals. All experiments are described in detail in our publication (91).

4.7 Establishment of Duox1 knockout HaCaT cell line via CRISPR-Cas9

To investigate the role of DUOX1 in the process detailed in the previous paragraph, we wanted to generate a specific antibody against DUOX1 because we could not find any commercially available one, that works properly in Western blot and immunostaining as well. To efficiently test the possible antibodies, *DUOX1* knockout HaCaT cell line was established by CRISPR-Cas9 technique. The success of the gene modification was first verified by Surveyor assay (Figure 15. A) and then by sequencing (Figure 15. B). Loss of a guanine and a cytosine nucleotide led to a frame-shift mutation and an early stop codon.

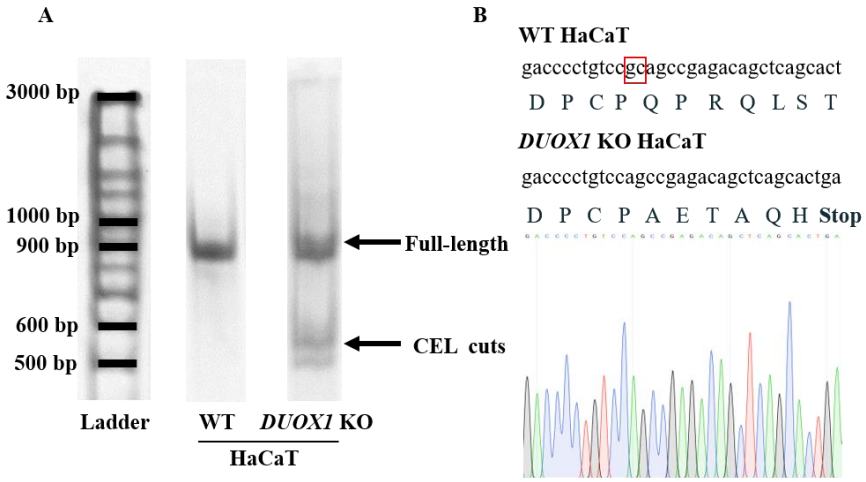

Figure 15. Verification of DUOX1 knockout HaCaT cell line. *(A) In Surveyor assay, due to the mutation in the DUOX1 KO sample, CEL enzyme cleavage products appeared. (B) Sequencing result. Two nucleotides were deleted, resulting in a frameshift mutation and an early stop codon.*

To confirm the lack of DUOX1 activity, H_2O_2 production was measured after different Ca^{2+} signal-generating stimuli, such as GSK 1016790A, ATPγS, and thapsigargin. H_2O_2 generation of HaCaT wild-type cells was significantly increased after the treatments, while stimulated *DUOX1* KO cells did not show any significant difference compared with the knockout control (Figure 16.).

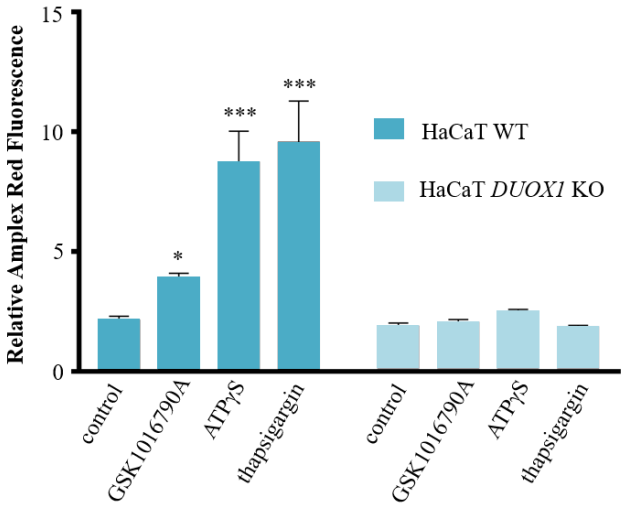

Figure 16. Measurement of H_2O_2 production with horseradish peroxidase and Amplex Red reagent. *HaCaT wild-type or CRISPR-modified DUOX1 knockout cells were stimulated with 2 nM GSK 1016790A or 10 μM ATPγS or 1 μM thapsigargin for 30 min.*

*Cumulative H_2O_2 production after 30 min normalized to initial H_2O_2 production. Representative plot of 3 independent experiments shows mean ± SD of triplicate. * p<0.05, *** p <0.001 compared with corresponding controls, by 2-way ANOVA. The figure is modified from Figure 2. of (91).*

To visualize the presence or lack of DUOX1 function, we applied a previously described technique (101) to set up a novel tyramide signal amplification-based assay. In the presence of DUOX1-produced H_2O_2, horseradish peroxidase (HRP) is able to convert a tyramide substrate into a highly reactive form that can covalently bind to tyrosine residues on proteins in the immediate proximity of H_2O_2 production. The biotinylated tyramide reagent is visualized through incubation with fluorescently labeled streptavidin. Using this technique, we can detect the DUOX1-dependent generation of H_2O_2 on a cultured monolayer of keratinocytes (Figure 17.).

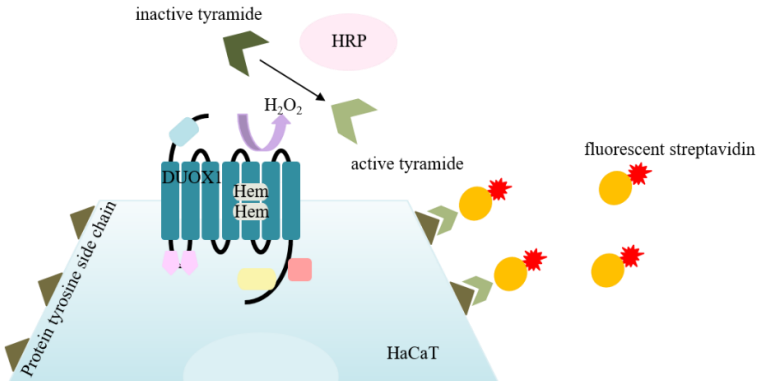

Figure 17. Schematic representation of biotinyl tyramide assay. *In the presence of DUOX1-generated H_2O_2, HRP covalently attaches activated, biotinylated tyramide to tyrosine side chains of cell surface proteins. The biotinylated tyramide reagent was detected through incubation with fluorescently labeled streptavidin.*

Biotinylated tyramide and HRP were added into the medium of thapsigargin-stimulated or non-stimulated wild-type or DUOX1-deficient HaCaT cells. The fluorescent streptavidin signal was detected by fluorescent microscope. At cell-cell borders of thapsigargin-stimulated wild-type cells, intense tyramide labeling was observed. Despite the treatment, no signal was detected in the absence of DUOX1 (Figure 18.).

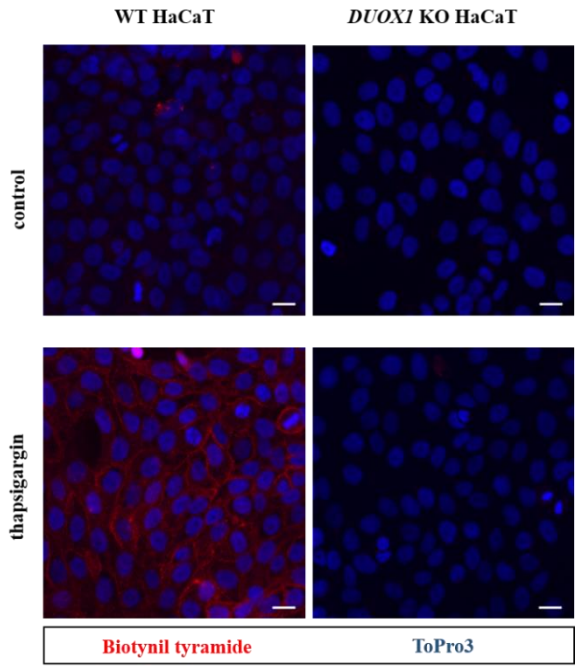

Figure 18. Biotinyl tyramide assay in HaCaT wild-type or CRISPR-modified Duox1 knockout cells. *Cells were treated with 1 µM thapsigargin in the presence or absence of horse radish peroxidase. The reaction solution also contained 27.5 µM biotinyl tyramide. After treatment, biotinylated molecules were labeled with fluorescent streptavidin and fixed. In addition, cell nuclei were stained with To-Pro-3. Scale bars: 10 µm. The experiment was repeated three times with similar results. The figure is modified from Figure 1. of (91).*

To summarize our results, we have established a DUOX1-deficient HaCaT cell line, which can be used to test antibodies against DUOX1.

4.8 Antibody development against human DUOX1

At the same time the *DUOX1* knockout HaCaT cell line was established, we started developing antibodies against human DUOX1. We chose a 411-amino-acids-long sequence of human DUOX1 to immunize New Zealand white rabbits. Thus, the antibody produced recognizes endogenous DUOX1 in HaCaT wild-type cells (Figure 19. A) and wild-type tissue lysate from mouse skin and bladder (Figure 19. B). The antibody was expected to recognize both the human and mouse samples because two species show a 91% amino acid identity and 96% similarity in this region of DUOX1. As a control for antibody specificity, *DUOX1* KO HaCaT or *Duox1* KO tissue was used. Antibody

recognizes DUOX1 properly in Western blot, but unfortunately, neither in immunohistochemistry nor immunocytochemistry.

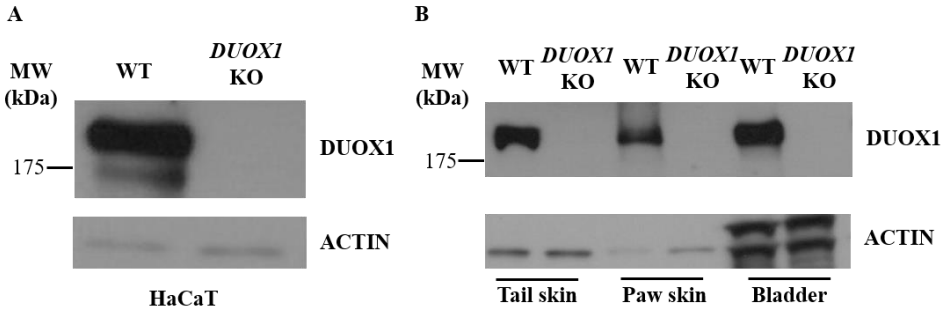

Figure 19. DUOX1 detection in Western blot with newly developed anti-DUOX1 antibody.

Western blot analysis of DUOX1 protein in HaCaT wild-type or CRISPR-modified DUOX1 knockout cells (A) or tail skin and hind paw skin and bladder from wild-type and Duox1 knockout mice. The Western blot was repeated three times with similar results.

4.9 Expression and activity of DUOX1 in mouse skin

After successfully developing an antibody, we returned to the original question and started investigating the role of DUOX1 in mouse skin. First, we wanted to confirm the presence of DUOX1 in the tissue. Therefore, we analyzed the expression of NADPH oxidase isoforms and their regulators in the mouse skin by quantitative reverse transcription PCR. *Duox1* was the most abundantly expressed NADPH oxidase isoform in the mouse tail and paw skin, and its maturation factor *DuoxA1* was also highly expressed (Figure 20.).

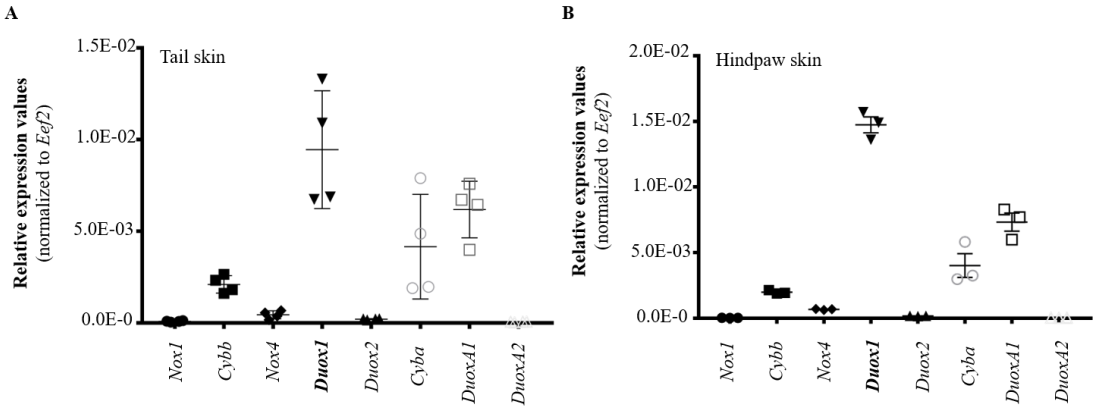

Figure 20. Quantitative PCR analysis of the expression of NADPH oxidase family components in mouse skin. *Dot plots represent mean ± SEM from 3-4 independent experiments. The figure is modified from Figure 1. of (91).*

We wanted to confirm our RNA results at the protein level as well. In wild-type tail and paw skin DUOX1 was successfully detected by Western blot. As control, DUOX1-deficient animal samples were used (Figure 21.).

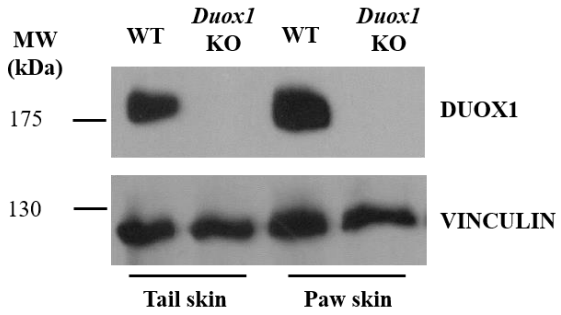

Figure 21. Western blot analysis of DUOX1 protein expression in mouse skin.
Detection of DUOX1 with Western blot in tail skin and hind paw skin tissue from wild-type and Duox1 knockout mice. The Western blot was repeated three times with similar results. The figure is modified from Figure 1. of (91).

Having demonstrated the presence of DUOX1 in mouse skin, we wanted to investigate its expression specifically in keratinocytes. Thus, we prepared primary mouse keratinocyte cell culture from the back skin of wild-type and *Duox1* KO mice. Then we successfully detected DUOX1 in keratinocytes by qPCR and Western blot (Figure 22.).

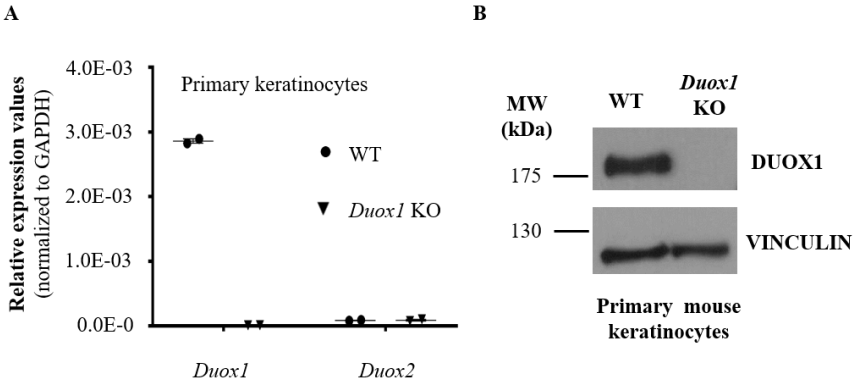

Figure 22. Expression of Duox1 in primary mouse keratinocytes. *(A) Quantitative PCR analysis of the expression of Duox1 and Duox2 in primary mouse keratinocytes from*

wild-type and Duox1 knockout mice. Dot plot represents mean ± SEM from 2 independent experiments. (B) Western blot analysis of DUOX1 protein in primary mouse keratinocytes from wild-type and Duox1 knockout mice. The Western blot was repeated three times with similar results. The figure is modified from Figure 1. of (91).

Last but not least, we also wanted to investigate protein activity, therefore we applied Amplex Red reagent to detect H_2O_2 production by primary mouse keratinocytes. Wild-type and *Duox1* KO cells were stimulated with GSK 1016790, and thapsigargin. While in the presence of DUOX1, there was a significant increase in H_2O_2 production, in the absence of the enzyme, the cells did not respond to the stimuli (Figure 23.).

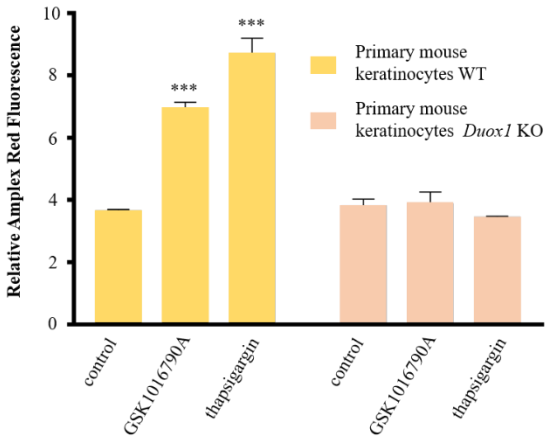

Figure 23. Measurement of Amplex Red fluorescence in wild-type and Duox1 knockout primary mouse keratinocytes. *Primary mouse back skin keratinocytes were stimulated with 2 nM GSK 1016790A or 100 nM thapsigargin for 30 minutes. Cumulative H_2O_2 production after 30 min normalized to initial H_2O_2 production. Representative plot of 3 independent experiments shows mean ± SD of triplicate. *** p <0.001 compared with corresponding controls by 2-way ANOVA. The figure is modified from Figure 2. of (91).*

4.10 Histological analysis of DUOX1-deficient mouse skin

After showing that DUOX1 is the predominant NADPH oxidase in mouse skin, we aimed to investigate the possible role of DUOX1 in the physiological sensory functions of the skin. We first analyzed histological sections of wild-type and *Duox1* KO mice. We wanted to determine if there is any observable change in the structure and differentiation of the mouse skin in the absence of DUOX1. We wanted to start with this histological analysis, as it has been previously described that the lack of DUOX1 in *C.elegans* leads

to severe morphological disorders of the cuticle (73, 102). I will not go into further details about the results because I was not involved in these experiments. To summarize, no structural or ultrastructural differences were found in the skin of DUOX1-deficient mice (91).

4.11 ATP release from stimulated keratinocytes

Keratinocytes express many distinct sensory and neurotransmitter receptors and can also be a source of cytokines, neurotrophic factors, neuropeptides, and neurotransmitters, which may mediate their contribution to nociceptive transduction (80). Adenosine-5′-triphosphate, one of the main extracellular signaling and neuromodulatory molecules, may be released from keratinocytes through several mechanisms, including temperature increase (80, 83, 103-105). Furthermore, isolated keratinocytes directly respond to mechanical stimulation by increasing $[Ca^{2+}]_{ic}$ (106-108). We assumed that stimuli that cause an increase in intracellular calcium concentrations would simultaneously activate DUOX1 and stimulate the release of ATP. We also wanted to observe if DUOX1 activity could modulate the secretion of mediators. We used a previously described, genetically encoded, GPCR activation-based ATP sensor, $GRAB_{ATP}$ (77) to answer these questions. This sensor construct is based on the insertion of a circularly permutated enhanced GFP (cpEGFP) into the ATP-binding $hP2Y_1$ receptor. The binding of ATP by this fusion construct specifically and sensitively enhances the fluorescence of cpEGFP. Wild-type or DUOX1 deficient HaCaT cells were cocultured with $GRAB_{ATP}$ expressing HEK293A cells and stimulated with 2.5 nM GSK 1016790A. We expected that if GSK 1016790A evokes ATP release then it should specifically activate the $GRAB_{ATP}$ sensors on the membrane of the transfected HEK293A cells. Indeed, after GSK 1016790A stimulation, we could repeatedly observe transient local oscillations followed by sustained high signals of extracellular ATP in the $GRAB_{ATP}$ expressing HEK293A cells. However, no obvious difference was detected between activation of sensor cells cocultured with wild-type or DUOX1-deficient HaCaT cells (Figure 24.). To confirm that GSK compound only affected keratinocytes and $GRAB_{ATP}$ expressing HEK293A cells did not respond to the stimulus, we also stimulated HEK cells in monoculture, however, no intensity change was observed (Figure 25.). Thus, we can conclude that the TRPV4 agonist generates intracellular calcium signal only in keratinocytes, leading to ATP release. We suggested that DUOX1-produced H_2O_2 might directly affect the $GRAB_{ATP}$ sensor. However, this

was also excluded when stimulating $GRAB_{ATP}$ expressing cells with H_2O_2, and no intensity change was detected (Figure 25.).

Thermal pain sensitivity can also be modulated by TRPV3-activatied prostaglandin release from keratinocytes (109). We compared the PGE2 -release of scrambled or *DUOX1*-specific siRNA-treated HaCaT cells, but there was no difference that could explain the enhanced thermal allodynic response previously displayed by the *Duox1* knockout mice (data not shown) (91).

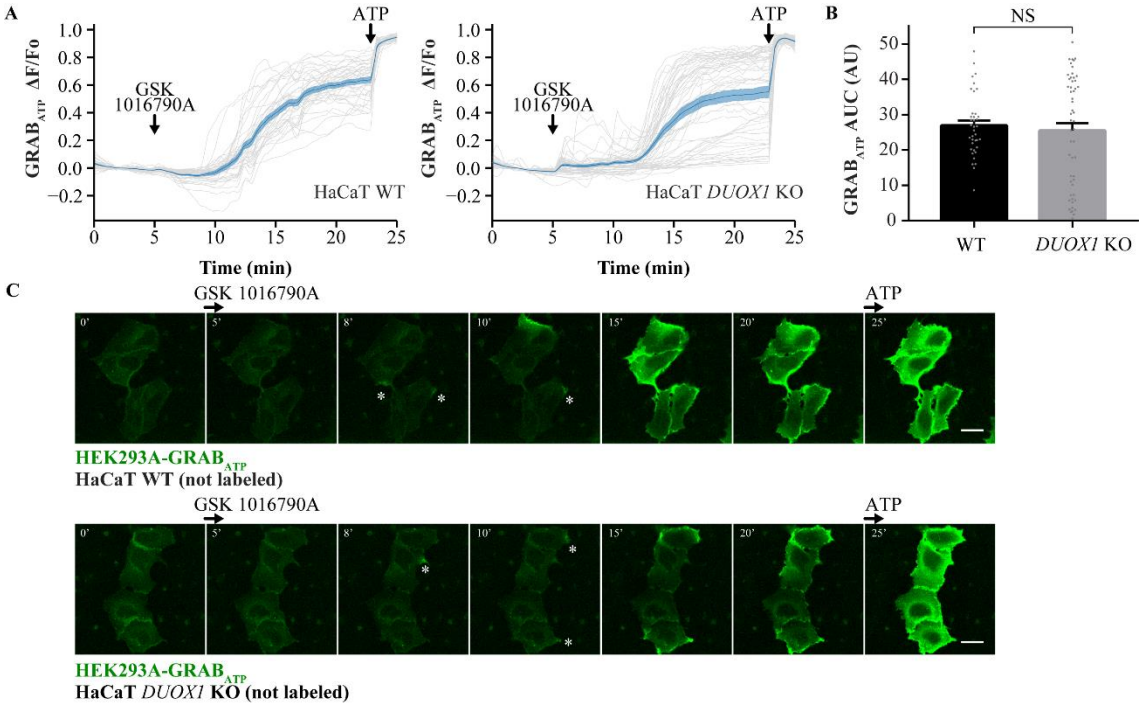

Figure 24. TRPV4 agonist, GSK 1016790A induced ATP secretion from wild-type and DUOX1 knockout HaCaT cells. *(A) Extracellular ATP-sensitive, fluorescent $GRAB_{ATP}$ sensor expressing HEK293A cells were cocultured with WT or DUOX1 knockout HaCaT. After a wash to remove any residual ATP in the media, the cells were treated with 2.5 nM GSK 1016790A and then with 1 μM ATP, as a positive control. Gray lines represent the normalized mean $GRAB_{ATP}$ intensity of every cell over time. Blue line shows the overall average of the normalized mean intensity of all the cells ± SEM (WT: n = 38, KO: n = 53 cells from 3 independent experiments). (B) The area under the curve (AUC) was measured for each cell during the time of the GSK 1016790A stimulus, between 5-27 min and was plotted per condition (mean ± SEM, gray dots represent values of individual cells). (C) Fluorescent images from different time points showing local oscillations*

(marked by asterisks) and sustained elevations of the GRAB$_{ATP}$ signal. Scale bars: 25 µm (91).

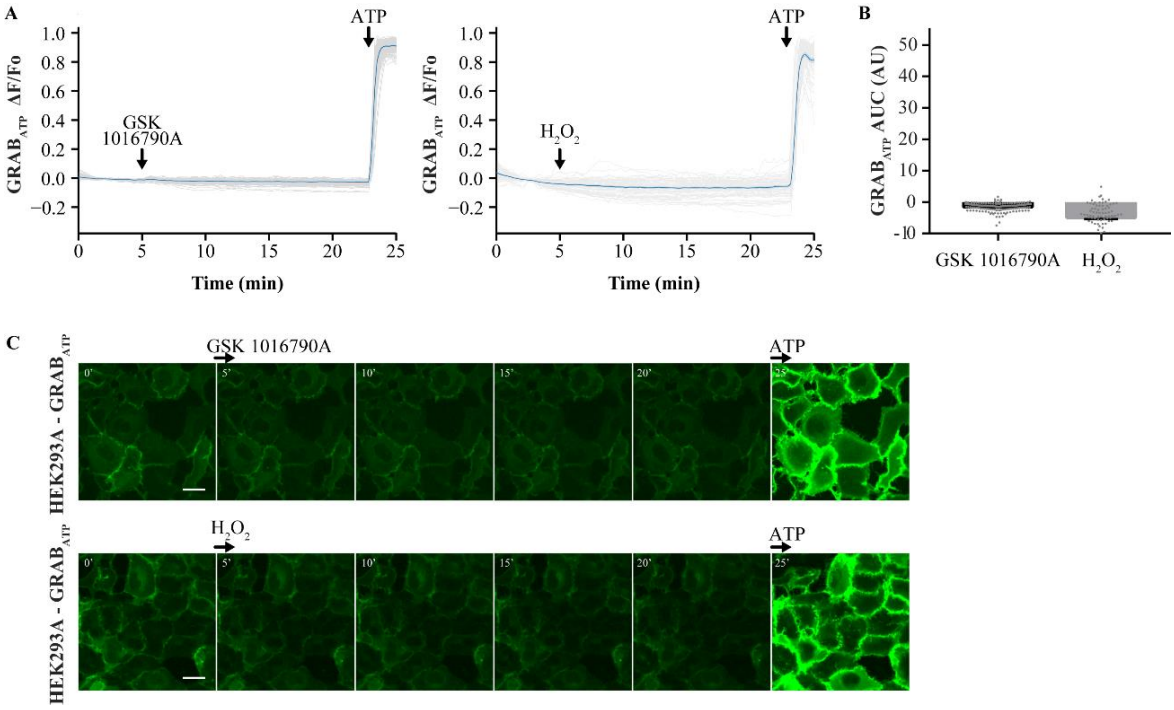

Figure 25. Neither GSK 1016790A nor H_2O_2 evokes ATP secretion from GRAB$_{ATP}$ sensor expressing HEK293A cells. *(A) After a wash to remove any residual ATP in the media, the cells were treated either with 2.5 nM GSK 1016790A or 500 µM H_2O_2 and then with 1 µM ATP, as a positive control. Gray lines represent the normalized mean GRAB$_{ATP}$ intensity of every cell over time. Blue line shows the overall average of the normalized mean intensity of all the cells ± SEM (GSK 1016790A: n = 149, H_2O_2: n = 83 cells from 3 independent experiments). (B) The area under the curve (AUC) was measured for each cell during the time of the GSK 1016790A and H_2O_2 stimulus, between 5-27 min, and was plotted per condition (mean ± SEM, gray dots represent values of individual cells). (C) Fluorescent images from different time points. Scale bars: 25 µm (91).*

4.12 Expression of TRP receptors and redox-sensitive ion channels in dorsal root ganglia and skin

After we did not detect a significant difference in the amount of mediators released from the stimulated keratinocytes, we analyzed the expression of the TRP receptor family in wild-type and *Duox1* knockout skin. We wanted to test that the previously described

behavioral phenotype changes were not due to a different TRP receptor expression pattern. As shown in Figure 26. A, among others expression of *Trpv3* and *Trpv4* were analyzed. These cation channels are activated by various distinct chemical and physical stimuli including warm temperatures. *Trpv3* is mainly expressed in the skin, and *Trpv4* is expressed in a wide range of tissues, such as primary sensory neurons and skin keratinocytes (110, 111). Both channels are involved in thermosensory function (112). We could not detect decisive differences between the wild-type and DUOX1-deficient samples.

After examining the keratinocytes and finding no explanation for our question, we turned our interest to DUOX1-produced H_2O_2. It is known that H_2O_2 can also act as a signaling molecule (74, 113). Therefore, we browsed the literature to find a possible target for DUOX1-produced H_2O_2. We hypothesized that the keratinocyte-derived H_2O_2 might also act on the primary sensory neuron. Therefore, we first confirmed available, detailed quantitative RNA- sequencing datasets of sensory ganglia (114). Only those ion channels and regulators of ion channels (dipeptidyl peptidase-like proteins) were analyzed, which have been previously described as redox-sensitive proteins. The expression pattern showed no difference between wild-type and *Duox1* knockout dorsal root ganglia (Figure 26. B). It is important to note that no *Duox1* or its maturation factor, *DuoxA1* was detectable in the DRG. We analyzed the expression of *Trpa1* and *Trpv1* as well. The TRPA1 receptor has been described on keratinocytes, and dorsal root ganglia (115). However, we could not detect it in the mouse skin (Figure 26. A), but it was present in the DRG, where it showed no difference between the wild-type and *Duox1* knockout samples (Figure 26. B). *Trpv1* is expressed in DRG sensory neurons and is involved in pain, thermoregulation, and pruritus (115). As shown in Figure 26. B we did not detect any DUOX1-dependent changes in the expression of this gene either.

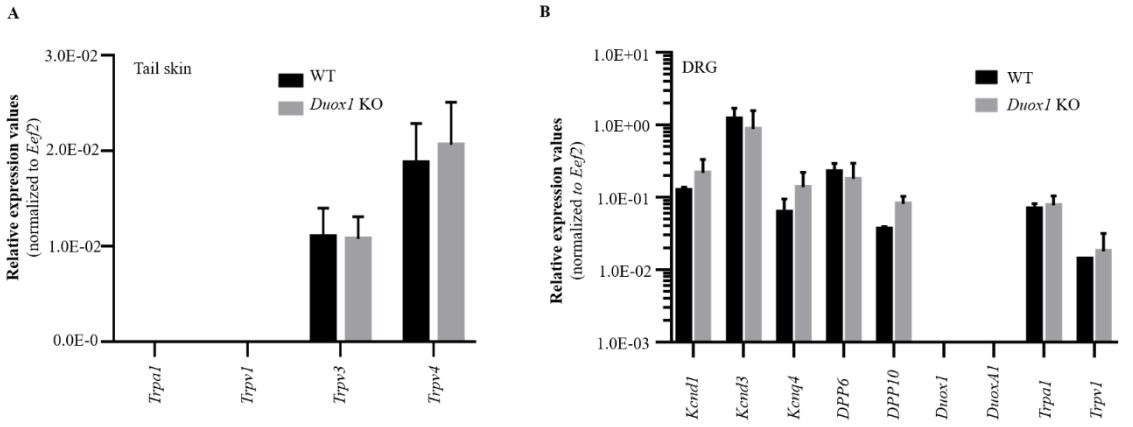

Figure 26. Expression of TRP receptors, ion channels and Duox1 in tail skin and dorsal root ganglion. *(A) Quantitative PCR analysis of the expression of TRP channels in mouse tail skin. Bars represent mean ± SEM from 2-4 independent experiments. (B) Quantitative PCR analysis of the expression of potassium channels, Duox1, DuoxA1, and TRP channels in wild-type and Duox1 knockout mouse dorsal root ganglion. Bars represent mean ± SEM from 2 independent experiments (91).*

4.13 H_2O_2-mediated redox changes of TRPA1-dependent intracellular calcium signal

After finding no difference in expression patterns, we started to investigate the redox sensitivity of the proteins. We first expressed recombinant TRPA1 channels in HEK293T cells, loaded them with calcium-sensitive fluorescent dye Fura-2-AM, and followed their intracellular calcium signals upon treatment with H_2O_2 and a TRPA1 agonist, AITC.

Following the addition of 100 or 500 µM H_2O_2, the TRPA1-expressing HEK cells - in contrast to the non-transfected cells - displayed an increase in intracellular calcium level (Figure 27. A, C). Additionally, after a 10-min pretreatment with H_2O_2, the AITC-evoked relative response was much smaller than in the non-pretreated cells (Figure 27. B, D). Consequently, H_2O_2 significantly affects the response of cells to allyl isothiocyanate. These results confirm the idea of keratinocyte-derived H_2O_2 acting as a paracrine mediator on TRPA1-expressing sensory nerve fibers.

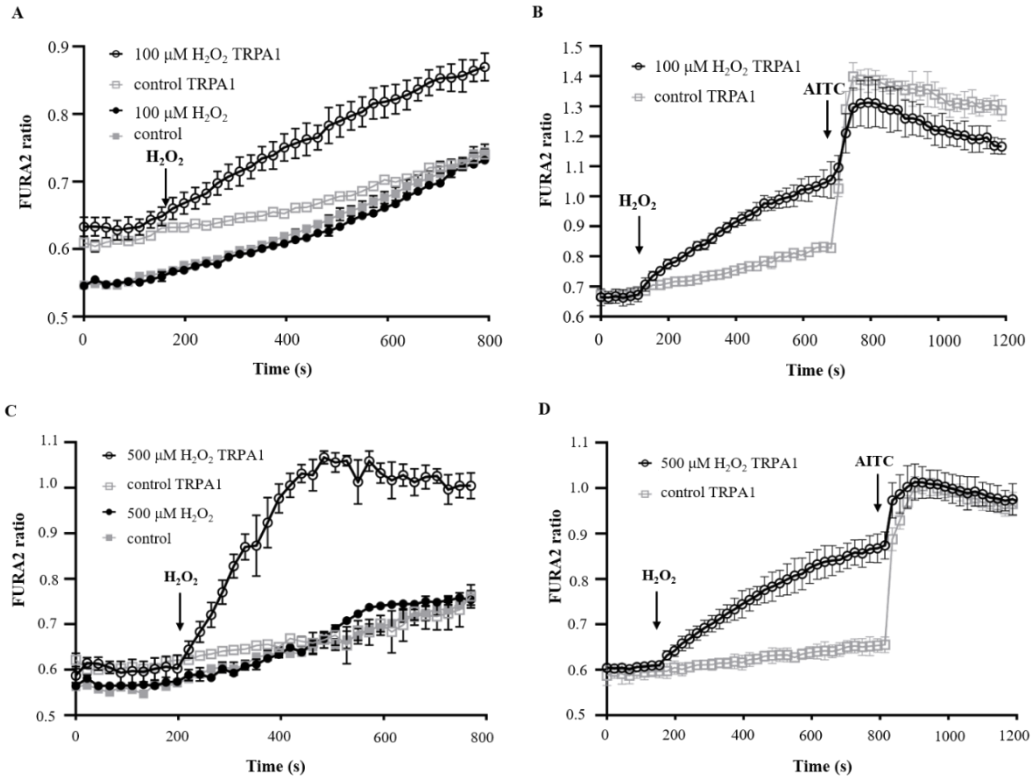

Figure 27. Ca^{2+} measurements with Fura-2-AM in HEK293 cells expressing TRPA1. *TRPA1-dependent effect of H_2O_2 on $[Ca^{2+}]_{ic}$. $[Ca^{2+}]_{ic}$ responses evoked by 100 µM (A) or 500 µM (C) H_2O_2 in the presence of TRPA1. (B) Change in $[Ca^{2+}]_{ic}$ of TRPA1 transfected HEK cells in response to sequential applications of 100 µM (B) or 500 µM (D) H_2O_2 and 10 µM AITC. Representative plot from at least 3 independent experiments shows the mean ± SD of triplicate. The figure is based on Figure S9. and Figure 8. of (91).*

4.14 Expression and H_2O_2 mediated redox changes of KCNQ4 potassium channel

Our next candidate for redox-sensitive ion channels was the voltage-gated M-type potassium channel, K7.4 or KCNQ4. Gamper *et al.* showed in a detailed electrophysiological study that the activity of this channel is enhanced by oxidative modification. Prolonged maintenance of the open state results in hyperpolarization and a decrease in the frequency of action potential firing (116). Using qPCR, we confirmed that *Kcnq4*, unlike *Duox1*, is indeed present in the DRG and in negligible amounts in the skin (Figure 28. A). In addition, *Duox1* was not detected in either the spinal cord or the brain (data not shown), suggesting that the enzyme is expressed only in keratinocytes and is not present in the sensory neural pathway (Figure 28. B).

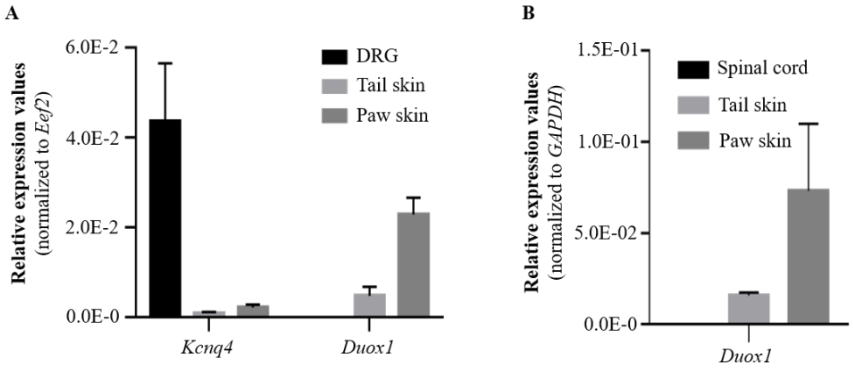

Figure 28. Expression of Kcnq4 and Duox1 in dorsal root ganglion, skin, and spinal cord. *(A) Quantitative PCR analysis of the Kcnq4 and Duox1 in wild-type mouse dorsal root ganglion, tail, and paw skin. (B) Expression of Duox1 in the spinal cord, tail, and paw skin. Bars represent mean ± SEM from 3 independent experiments. The figure is modified from Figure 9. of (91).*

Next, we wanted to confirm the redox sensitivity of Kcnq4. In this experiment, biotinylated iodoacetamide was used to alkylate the cysteine thiol groups of the potassium channel. If KCNQ4 bound BIAM, it could be detected by streptavidin-HRP on Western blot. However, if the thiol reacted with H_2O_2, it could no longer bind BIAM and no signal was detected (Figure 29.).

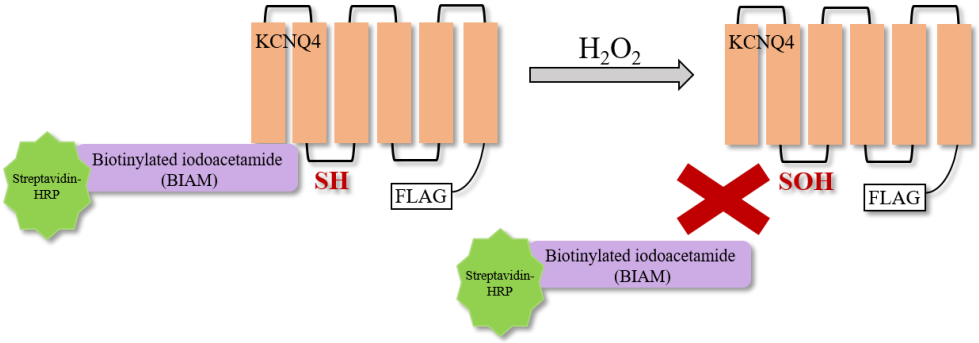

Figure 29. Schematic representation of detection of cysteine redox state in KCNQ4. *The thiol side chain in the cysteine of KCNQ4 can be alkylated using biotinylated iodoacetamide (BIAM). Binding of the channel to BIAM can be detected on a Western blot using streptavidin-HRP. However, if the thiol reacts with H_2O_2, it loses its ability to bind BIAM and the biotin signal cannot be detected on a Western blot.*

Therefore, we transfected HEK293 cells with FLAG-tagged, recombinant *Kcnq4* and stimulated with increasing concentrations of H_2O_2, followed by cell lysis in BIAM-containing buffer. After that KCNQ4 was immunoprecipitated by monoclonal anti-FLAG

antibody and we ran the immunoprecipitate on SDS polyacrylamide gel to test the amount of biotin labeling with streptavidin-HRP. As it is shown in Figure 30. A, the higher concentration of H_2O_2 was used, the weaker the biotin signal is, because oxidized protein can not bind BIAM and streptavidin-HRP. As a loading control we used antibody against FLAG.

To confirm these results, and examine the reversibility of oxidation we also carried out a reverse BIAM labeling. In this case, after the H_2O_2 treatment, we first alkylated the non-oxidized KCNQ4 with N-ethyl-maleimide, then we reduced all the reversibly oxidized molecules with dithiothreitol, and finally, we labeled these reduced molecules with BIAM, then proceeded as in the previous experiment. This way the biotin signal is linearly proportional to the amount of oxidation. As a loading control we used antibody against FLAG again (Figure 30. B).

These results demonstrated that *Kcnq4* is expressed in DRGs but not in keratinocytes and is indeed a direct molecular target of H_2O_2-mediated redox changes.

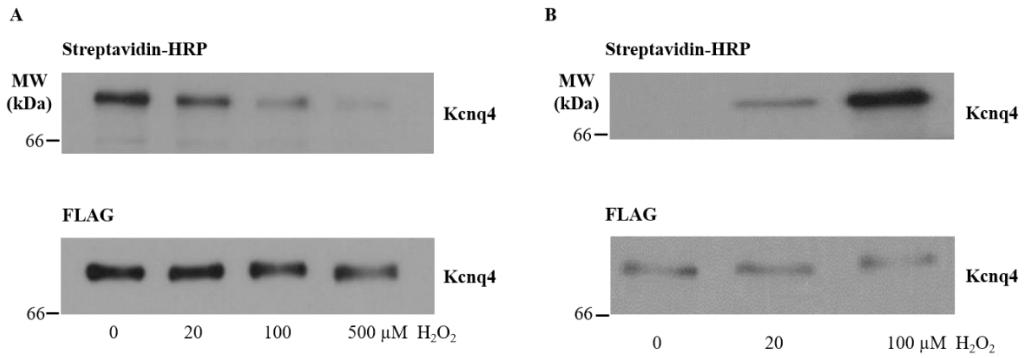

Figure 30. H_2O_2 mediated redox changes of the voltage-gated potassium channel, KCNQ4. *(A) HEK293 cells expressing FLAG-tagged KCNQ4 were treated with H_2O_2 (0, 20, 100, 500 µM) and lysed in the presence of BIAM. Following anti-FLAG immunoprecipitation, BIAM signal was detected by streptavidin-HRP on western blot. (B) After H_2O_2 treatment (0, 20, 100 µM), non-oxidized thiols were alkylated with N-ethylmaleimide, then lysates were reduced with dithiothreitol and labeled with BIAM. We continued with anti-FLAG immunoprecipitation and streptavidin-HRP detection. The experiment was repeated five times with similar results. The figure is modified from Figure 9. of (91).*

5. Discussion

Bae *et al.* were the first to report the production of H_2O_2 induced by epidermal growth factor in A431 cells (94). Subsequent studies have confirmed this finding (117, 118). Paulsen *et al.* identified the phagocytic NADPH oxidase, NOX2, as the source of EGF-evoked ROS generation in A431 cells (119). We also confirmed that epidermal growth factor enhances H_2O_2 production in A431 and HaCaT cells. However, we did not detect the presence of NOX2 in any of the cell lines, nor the presence of additional subunits required for phagocytic oxidase function. Based on our results, we have identified another NADPH oxidase, DUOX1, as the long-sought source of EGF-induced H_2O_2 production in epidermal cells. The presence of this enzyme in A431 and HaCaT was confirmed at both RNA and protein levels. We showed that the activation of DUOX1 in these cells is a consequence of EGF-induced elevation of intracellular calcium levels. We also demostrated that knockdown or knockout of DUOX1 eliminates the EGF-induced ROS production. Our experiments also showed that several reagents with varying mechanisms of action can stimulate DUOX1-dependent H_2O_2 production in a calcium-dependent manner, indicating that calcium signals generated in keratinocytes ultimately lead to increased H_2O_2 release.

Kwon *et al.* suggested that H_2O_2 production by calcium-activated DUOX1 acts in a positive feedback loop, which leads to augmented release of Ca^{2+} from the ER and subsequent influx of extracellular Ca^{2+} in Jurkat cells (69). However, Donkó *et al.* did not detect such mechanism in urothelial cells (66), nor did we in A431 and HaCaT cells.

It was observed that EGF-induced H_2O_2 might enhance tyrosine phosphorylation of proteins through the inhibition of protein tyrosine phosphatases (98, 99). We also investigated this potential role of DUOX1-produced H_2O_2. However, we did not observe a significant change in the overall tyrosine phosphorylation pattern when DUOX1 expression was repressed. Therefore, our results suggest that protein tyrosine phosphatases are not targets of DUOX1-generated H_2O_2. However, it is possible that our experiments missed subtle changes in phosphorylation or phosphorylation changes of specific targets. In order to analyze the possible relationship between DUOX1 and other growth factor signaling pathways, we examined the effects of VEGF and IGF-1. Previous studies suggest that HaCaT cells express receptors for both ligands (120, 121). Our findings indicate that neither IGF-1 nor VEGF led to as significant an increase in

intracellular calcium as EGF. Consequently, we could not detect significant H_2O_2 production following IGF-1 or VEGF stimulation (data not shown). We conclude that the co-presence of a specific growth factor-induced calcium signal and DUOX1 activity is required to detect growth factor-induced H_2O_2 production. Our workgroup identified a molecular target of EGF-induced DUOX1-dependent H_2O_2 production and found evidence that DUOX1-derived H_2O_2 leads to an oxidative shift in the redox state of the peroxiredoxin-thioredoxin system in HaCaT cells (74). Although our experiments showed that H_2O_2 is released into the extracellular space, it is possible that Aquaporin facilitates the uptake of H_2O_2 into mammalian cells, resulting in downstream intracellular signaling, as previously suggested by Miller *et al.* (122). In the cytosol, H_2O_2 directly reacts with Prx I and Prx II, leading to the oxidation of Trx during the regeneration of peroxiredoxins. The protein interactions of Trx are influenced by its oxidative state, which means that the indirect oxidation of Trx by DUOX1 may impact signaling pathways regulated by thioredoxin-interacting proteins (123).

Furthermore, Sobotta *et al.* demonstrated that Prx II operates as a redox relay with the transcription factor STAT3, resulting in the formation of disulfide-linked STAT3 oligomers with decreased transcriptional activity (124). This suggests that peroxiredoxins are more than just antioxidants and actively participate in signaling. It is plausible that activation of DUOX1 represents a signaling step before the PRX II-STAT3 interaction.

Although detailed information is available on the structure of DUOX1, there is still relatively limited knowledge about the physiological functions and biochemical mechanisms the enzyme is involved in (6, 29). DUOX1 is a transmembrane NADPH oxidase initially discovered with DUOX2 in the thyroid gland (24, 25). While the role of DUOX2 in thyroid hormone biosynthesis is well-established, the absence of DUOX1 does not affect hormone synthesis of the thyroid gland in mice. Loss of function of *DUOX2* and its maturation factor *DUOXA2* leads to congenital hypothyroidism. In contrast, DUOX1-deficient mice do not develop hypothyroidism (4).

Subsequent studies showed that the expression of DUOX enzymes is not restricted to the thyroid gland but they are also present in several epithelial cells (40, 44, 45, 54). The precise function of the enzymes in various locations is still not fully comprehended, but prior research has identified diverse potential roles. For instance, DUOX enzymes were observed to play a part in respiratory epithelial cell wound healing, cellular responses to

allergic and microbial triggers (50, 60, 125, 126), and host defense in *Drosophila melanogaster* (127). Furthermore, DUOX1 is highly expressed in the bladder epithelium, where antimicrobial activity seems less plausible. Instead, it is suggested to play a role in mechanotransduction. In primary keratinocytes, IL-4/IL-13-induced DUOX1 enhanced STAT6 phosphorylation via oxidative inactivation of PTP1B (38).

We examined the expression and activity of NADPH oxidases in mouse skin and primary keratinocytes and confirmed that DUOX1 is the most abundant isoform in these samples. We generated a specific polyclonal antibody against DUOX1 and demonstrated its expression at the protein level. By devising a new fluorescent microscope-based technique, we were able to visualize enzymatic H_2O_2 production in cell culture. To further investigate the role of DUOX1 in the skin, we studied DUOX1-deficient mice. Interestingly, Choe *et al.* observed that the amount of various differentiation markers such as loricrin and keratin-10 is reduced at RNA level upon knockdown of *DUOX1* by RNA interference in primary keratinocytes (71). However, we could not confirm this at the protein level when we examined the skin of DUOX1-deficient mice using fluorescent immunostaining. It has also been shown that DUOX (Ce-DUOX1) plays an essential role in stabilizing the cuticular extracellular matrix of *C. elegans* by catalyzing the cross-linking of tyrosine residues (73). Nevertheless, we have not discovered any differences in the structure or ultrastructure of skin in DUOX1-deficient animals.

The epidermis, the outermost layer of the skin, comprises a stratified squamous epithelium of mainly keratinocytes. It has been conventionally believed that keratinocytes are exclusively responsible for the physical and chemical barrier. In contrast, sensory neurons serve as the only detectors and transducers of noxious thermal, mechanical, or chemical stimuli through their end branches that pass between keratinocytes - the intraepidermal free nerve endings (FNEs). In the last two decades, however, the sensory role of keratinocytes has been discovered, for example, in inflammatory pain or innocuous and noxious touch (77, 105, 128). Furthermore, it has been described that epidermal keratinocytes interact with sensory neurons through *en passant* synaptic-like connections (79). Based on the literature data, several sensory tests were performed in *Duox1* knockout animals. DUOX1-deficient mice were significantly sensitized to thermal stimuli compared to wild-type animals after allyl isothiocyanate pretreatment. Additionally, *Duox1* knockout mice displayed enhanced nocifensive responses following

intraplantar formalin injection. Conversely, there was no variation in mechanonociceptive thresholds. These findings suggest an altered sensitivity of peripheral nerve endings in the skin, as indicated by the selective difference in nocifensive behavior towards thermal stimuli. These results are aligned with the observation that mechanical and thermal hyperalgesia are controlled differently in the central nervous system (129).

We showed that *Duox1* is present only in the keratinocyte and not in the sensory nerve endings. We examined receptors involved in thermal nociception expressed on keratinocytes and found no significant differences at the RNA level. To investigate further, we looked into mediators released from keratinocytes and hypothesized that DUOX1-produced H_2O_2 might influence the release of signaling molecules from keratinocytes in an autocrine fashion. Various mediators, such as ATP, prostaglandins, leukotrienes, TNF-α, interleukins, and endogenous opioids have been reported to be released from keratinocytes (130-133). We specifically studied the release of PGE2 and ATP, which are known to induce nociceptive responses, but found no difference between wild-type and DUOX1-deficient keratinocytes. However, we cannot rule out that the activity of DUOX1 affects the secretion of other mediators.

We assumed that DUOX1-produced H_2O_2 might be a paracrine mediator of nociceptive signaling. Therefore, we browsed the literature for redox-sensitive cell surface proteins expressed on sensory nerve fibers. TRPA1 and KCNQ4 were selected for further analysis. Consistent with previous studies, H_2O_2 could induce calcium signals in cells expressing TRPA1 (134). Interestingly, pretreatment of TRPA1-expressing cells with H_2O_2 decreased their sensitivity to TRPA1 agonists. This finding suggests that H_2O_2 desensitizes sensory nerves, attenuating their responsiveness to nociceptive stimuli. A different perspective on the impact of H_2O_2 is that it reduces the contrast between the non-stimulated and AITC-stimulated conditions, ultimately resulting in a decreased S/S0 ratio in the Weber-Fechner equation. As a result, the just noticeable difference, or the smallest detectable change in stimuli, is increased.

Furthermore, we provided biochemical evidence that KCNQ4 undergoes H_2O_2-mediated oxidation at concentrations as low as 20 µM H_2O_2. Slower closure of KCNQ4 channels following ROS exposure may also contribute to slower or reduced peripheral activation of sensory nerve fibers. The co-expression of KCNQ4 and TRPA1 in DRG cell

populations is currently unknown. It is unclear whether these channels are present in the same or separate populations (Figure 31.).

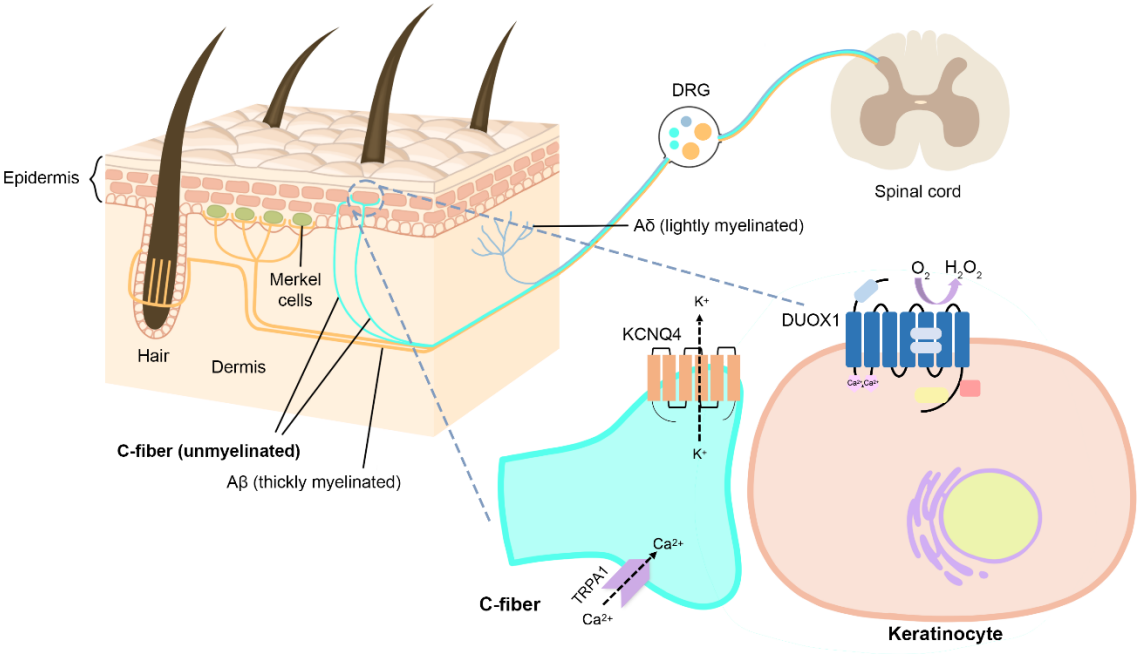

Figure 31. Schematic diagram depicting the proposed mechanism of function of DUOX1 in nociception.

Our findings suggest that ROS may have a subtle yet important regulatory function in sensory processes. This is a departure from the conventional understanding of ROS as a pain amplifying factor (135, 136). The key distinction in the interpretation of the role of ROS likely stems from the source and control of ROS release. The substantial ROS production by leukocytes that infiltrate tissues during injury or significant inflammation differs greatly from the constant, low-level physiological ROS production by keratinocytes in the undamaged epidermis.

Taken together, we have demonstrated the presence of DUOX1 in keratinocytes, and our results reveal a previously unrecognized physiological sensory function of DUOX1 in the skin. We also confirmed that several stimuli enhanced the activity of the enzyme in a calcium-dependent manner. This observation also raises the possibility that DUOX1 is involved in sensing various stimuli from the outside world, which trigger an increase in intracellular calcium levels in keratinocytes. Furthermore, our findings on ROS released from keratinocytes might provide a novel insight into the nociceptive and analgesic signaling pathways in the skin.

6. Conclusions

Based on our objectives and the results described above, the following conclusions can be drawn:

1. Dual Oxidase 1 is the source of the epidermal growth factor-induced H_2O_2 production in squamous cells.

2. Other mediators (niacin, ATPγS, TRPV4-agonist) can also activate DUOX1.

3. DUOX1 is the most abundant NADPH oxidase in A431, HaCaT cells and mouse keratinocytes.

4. The amount of PGE2 and ATP released from keratinocytes was found to be similar in both wild-type and DUOX1-deficient keratinocytes.

5. We identified TRPA1 and KCNQ4 as potential targets of DUOX1-produced H_2O_2, which might explain the altered nociceptive behavior of DUOX1-deficient mice.

7. Summary

NADPH oxidases are major sources for regulated production of reactive oxygen species in mammalian cells. Dual Oxidase 1 (DUOX1), a membrane protein that produces H_2O_2, is a member of this family and is highly expressed in epithelial cells, such as airways, bladder, and skin. However, its physiological role is yet poorly understood. Therefore, our work aimed to understand its function in squamous cells better.

As DUOX1-specific, reliable antibodies were not commercially available, we developed a polyclonal antibody against human DUOX1 and generated a *DUOX1* knockout HaCaT cell line using CRISPR-Cas9 technique. As a result of our experiments, we showed that among the seven isoforms, DUOX1 is the predominant NADPH oxidase in epidermoid tumor cells, spontaneously immortalized human HaCaT keratinocytes and also in the mouse skin. Furthermore, we demonstrated that epidermal growth factor stimulates H_2O_2 production in keratinocytes exclusively through DUOX1 activation in a calcium-dependent manner. We also described additional stimuli that activate ROS generation of the enzyme. However, the production of H_2O_2 by DUOX1 does not impact the intracellular calcium level.

To better understand the role of Dual Oxidase 1 in the skin, we also used DUOX1-deficient mice. Our research aimed to investigate the reason behind the increased sensitivity to thermal stimuli in *Duox1* knockout mice following pretreatment with TRPA1 agonist allyl isothiocyanate. After examining the structure and differentiation of the skin and finding no abnormalities that could explain the observed phenomenon, we investigated keratinocyte receptors and released mediators in more detail. No significant differences were found here, so we focused on possible molecular targets of DUOX1-produced H_2O_2. We identified two redox-sensitive proteins, TRPA1 and KCNQ4, which are expressed in the dorsal root ganglion and might play a role in the behavioral response of DUOX1-deficient animals to thermal stimuli.

Our work showed distinct physiological stimuli that activate DUOX1 in squamous cells. We further investigated and characterized the role of the enzyme in the skin and identified molecular targets of H_2O_2, leading to a more comprehensive understanding of Dual Oxidase 1.

8. References

1. Li R, Jia Z, Trush MA. Defining ROS in Biology and Medicine. React Oxyg Species (Apex). 2016;1(1):9-21.
2. Checa J, Aran JM. Reactive Oxygen Species: Drivers of Physiological and Pathological Processes. J Inflamm Res. 2020;13:1057-1073.
3. Lambeth JD, Neish AS. Nox enzymes and new thinking on reactive oxygen: a double-edged sword revisited. Annu Rev Pathol. 2014;9:119-145.
4. Buvelot H, Jaquet V, Krause KH. Mammalian NADPH Oxidases. Methods Mol Biol. 2019;1982:17-36.
5. De Deken X, Corvilain B, Dumont JE, Miot F. Roles of DUOX-mediated hydrogen peroxide in metabolism, host defense, and signaling. Antioxid Redox Signal. 2014;20(17):2776-2793.
6. Ogboo BC, Grabovyy UV, Maini A, Scouten S, van der Vliet A, Mattevi A, Heppner DE. Architecture of the NADPH oxidase family of enzymes. Redox Biol. 2022;52:102298.
7. Bedard K, Krause KH. The NOX family of ROS-generating NADPH oxidases: physiology and pathophysiology. Physiol Rev. 2007;87(1):245-313.
8. Baehner RL, Karnovsky ML. Deficiency of reduced nicotinamide-adenine dinucleotide oxidase in chronic granulomatous disease. Science. 1968;162(3859):1277-1279.
9. Buvelot H, Posfay-Barbe KM, Linder P, Schrenzel J, Krause KH. Staphylococcus aureus, phagocyte NADPH oxidase and chronic granulomatous disease. FEMS Microbiol Rev. 2017;41(2):139-157.
10. Suh YA, Arnold RS, Lassegue B, Shi J, Xu X, Sorescu D, Chung AB, Griendling KK, Lambeth JD. Cell transformation by the superoxide-generating oxidase Mox1. Nature. 1999;401(6748):79-82.
11. Hayes P, Dhillon S, O'Neill K, Thoeni C, Hui KY, Elkadri A, Guo CH, Kovacic L, Aviello G, Alvarez LA, Griffiths AM, Snapper SB, Brant SR, Doroshow JH, Silverberg MS, Peter I, McGovern DP, Cho J, Brumell JH, Uhlig HH, Bourke B, Muise AA, Knaus UG. Defects in NADPH Oxidase Genes NOX1 and DUOX2 in Very Early Onset Inflammatory Bowel Disease. Cell Mol Gastroenterol Hepatol. 2015;1(5):489-502.

12. Schwerd T, Bryant RV, Pandey S, Capitani M, Meran L, Cazier JB, Jung J, Mondal K, Parkes M, Mathew CG, Fiedler K, McCarthy DJ, Consortium WGS, Oxford IBDcsi, investigators CiIg, Consortium UIG, Sullivan PB, Rodrigues A, Travis SPL, Moore C, Sambrook J, Ouwehand WH, Roberts DJ, Danesh J, Study I, Russell RK, Wilson DC, Kelsen JR, Cornall R, Denson LA, Kugathasan S, Knaus UG, Serra EG, Anderson CA, Duerr RH, McGovern DP, Cho J, Powrie F, Li VS, Muise AM, Uhlig HH. NOX1 loss-of-function genetic variants in patients with inflammatory bowel disease. Mucosal Immunol. 2018;11(2):562-574.
13. Esworthy RS, Kim BW, Chow J, Shen B, Doroshow JH, Chu FF. Nox1 causes ileocolitis in mice deficient in glutathione peroxidase-1 and -2. Free Radic Biol Med. 2014;68:315-325.
14. Sirokmany G, Donko A, Geiszt M. Nox/Duox Family of NADPH Oxidases: Lessons from Knockout Mouse Models. Trends Pharmacol Sci. 2016;37(4):318-327.
15. Kikuchi H, Hikage M, Miyashita H, Fukumoto M. NADPH oxidase subunit, gp91(phox) homologue, preferentially expressed in human colon epithelial cells. Gene. 2000;254(1-2):237-243.
16. Paffenholz R, Bergstrom RA, Pasutto F, Wabnitz P, Munroe RJ, Jagla W, Heinzmann U, Marquardt A, Bareiss A, Laufs J, Russ A, Stumm G, Schimenti JC, Bergstrom DE. Vestibular defects in head-tilt mice result from mutations in Nox3, encoding an NADPH oxidase. Genes Dev. 2004;18(5):486-491.
17. Banfi B, Malgrange B, Knisz J, Steger K, Dubois-Dauphin M, Krause KH. NOX3, a superoxide-generating NADPH oxidase of the inner ear. J Biol Chem. 2004;279(44):46065-46072.
18. Geiszt M, Kopp JB, Varnai P, Leto TL. Identification of renox, an NAD(P)H oxidase in kidney. Proc Natl Acad Sci U S A. 2000;97(14):8010-8014.
19. Shiose A, Kuroda J, Tsuruya K, Hirai M, Hirakata H, Naito S, Hattori M, Sakaki Y, Sumimoto H. A novel superoxide-producing NAD(P)H oxidase in kidney. J Biol Chem. 2001;276(2):1417-1423.
20. Banfi B, Molnar G, Maturana A, Steger K, Hegedus B, Demaurex N, Krause KH. A Ca(2+)-activated NADPH oxidase in testis, spleen, and lymph nodes. J Biol Chem. 2001;276(40):37594-37601.

21. Cheng G, Cao Z, Xu X, van Meir EG, Lambeth JD. Homologs of gp91phox: cloning and tissue expression of Nox3, Nox4, and Nox5. Gene. 2001;269(1-2):131-140.
22. Touyz RM, Anagnostopoulou A, Rios F, Montezano AC, Camargo LL. NOX5: Molecular biology and pathophysiology. Exp Physiol. 2019;104(5):605-616.
23. Petheo GL, Kerekes A, Mihalffy M, Donko A, Bodrogi L, Skoda G, Barath M, Hoffmann OI, Szeles Z, Balazs B, Sirokmany G, Fabian JR, Toth ZE, Baksa I, Kacskovics I, Hunyady L, Hiripi L, Bosze Z, Geiszt M. Disruption of the NOX5 Gene Aggravates Atherosclerosis in Rabbits. Circ Res. 2021;128(9):1320-1322.
24. Dupuy C, Ohayon R, Valent A, Noel-Hudson MS, Deme D, Virion A. Purification of a novel flavoprotein involved in the thyroid NADPH oxidase. Cloning of the porcine and human cdnas. J Biol Chem. 1999;274(52):37265-37269.
25. De Deken X, Wang D, Many MC, Costagliola S, Libert F, Vassart G, Dumont JE, Miot F. Cloning of two human thyroid cDNAs encoding new members of the NADPH oxidase family. J Biol Chem. 2000;275(30):23227-23233.
26. Pachucki J, Wang D, Christophe D, Miot F. Structural and functional characterization of the two human ThOX/Duox genes and their 5'-flanking regions. Mol Cell Endocrinol. 2004;214(1-2):53-62.
27. Donko A, Peterfi Z, Sum A, Leto T, Geiszt M. Dual oxidases. Philos Trans R Soc Lond B Biol Sci. 2005;360(1464):2301-2308.
28. Sun J. Structures of mouse DUOX1-DUOXA1 provide mechanistic insights into enzyme activation and regulation. Nat Struct Mol Biol. 2020;27(11):1086-1093.
29. Wu JX, Liu R, Song K, Chen L. Structures of human dual oxidase 1 complex in low-calcium and high-calcium states. Nat Commun. 2021;12(1):155.
30. Rigutto S, Hoste C, Grasberger H, Milenkovic M, Communi D, Dumont JE, Corvilain B, Miot F, De Deken X. Activation of dual oxidases Duox1 and Duox2: differential regulation mediated by camp-dependent protein kinase and protein kinase C-dependent phosphorylation. J Biol Chem. 2009;284(11):6725-6734.
31. Grasberger H, Refetoff S. Identification of the maturation factor for dual oxidase. Evolution of an eukaryotic operon equivalent. J Biol Chem. 2006;281(27):18269-18272.

32. Morand S, Ueyama T, Tsujibe S, Saito N, Korzeniowska A, Leto TL. Duox maturation factors form cell surface complexes with Duox affecting the specificity of reactive oxygen species generation. FASEB J. 2009;23(4):1205-1218.
33. Carvalho DP, Dupuy C. Thyroid hormone biosynthesis and release. Mol Cell Endocrinol. 2017;458:6-15.
34. Liu S, Han W, Zang Y, Zang H, Wang F, Jiang P, Wei H, Liu X, Wang Y, Ma X, Ge Y. Identification of Two Missense Mutations in DUOX1 (p.R1307Q) and DUOXA1 (p.R56W) That Can Cause Congenital Hypothyroidism Through Impairing H(2)O(2) Generation. Front Endocrinol (Lausanne). 2019;10:526.
35. Aycan Z, Cangul H, Muzza M, Bas VN, Fugazzola L, Chatterjee VK, Persani L, Schoenmakers N. Digenic DUOX1 and DUOX2 Mutations in Cases With Congenital Hypothyroidism. J Clin Endocrinol Metab. 2017;102(9):3085-3090.
36. Nie Y, Speakman JR, Wu Q, Zhang C, Hu Y, Xia M, Yan L, Hambly C, Wang L, Wei W, Zhang J, Wei F. ANIMAL PHYSIOLOGY. Exceptionally low daily energy expenditure in the bamboo-eating giant panda. Science. 2015;349(6244):171-174.
37. Harper RW, Xu C, Eiserich JP, Chen Y, Kao CY, Thai P, Setiadi H, Wu R. Differential regulation of dual NADPH oxidases/peroxidases, Duox1 and Duox2, by Th1 and Th2 cytokines in respiratory tract epithelium. FEBS Lett. 2005;579(21):4911-4917.
38. Hirakawa S, Saito R, Ohara H, Okuyama R, Aiba S. Dual oxidase 1 induced by Th2 cytokines promotes STAT6 phosphorylation via oxidative inactivation of protein tyrosine phosphatase 1B in human epidermal keratinocytes. J Immunol. 2011;186(8):4762-4770.
39. Wu Y, Antony S, Juhasz A, Lu J, Ge Y, Jiang G, Roy K, Doroshow JH. Up-regulation and sustained activation of Stat1 are essential for interferon-gamma (IFN-gamma)-induced dual oxidase 2 (Duox2) and dual oxidase A2 (DuoxA2) expression in human pancreatic cancer cell lines. J Biol Chem. 2011;286(14):12245-12256.
40. Geiszt M, Witta J, Baffi J, Lekstrom K, Leto TL. Dual oxidases represent novel hydrogen peroxide sources supporting mucosal surface host defense. FASEB J. 2003;17(11):1502-1504.

41. Zeldow BJ. Studies on the antibacterial action of human saliva. III. Cofactor requirements of Lactobacillus bactericidin. J Immunol. 1963;90:12-16.
42. Klebanoff SJ, Clem WH, Luebke RG. The peroxidase-thiocyanate-hydrogen peroxide antimicrobial system. Biochim Biophys Acta. 1966;117(1):63-72.
43. Fischer H, Gonzales LK, Kolla V, Schwarzer C, Miot F, Illek B, Ballard PL. Developmental regulation of DUOX1 expression and function in human fetal lung epithelial cells. Am J Physiol Lung Cell Mol Physiol. 2007;292(6):L1506-1514.
44. Schwarzer C, Machen TE, Illek B, Fischer H. NADPH oxidase-dependent acid production in airway epithelial cells. J Biol Chem. 2004;279(35):36454-36461.
45. Forteza R, Salathe M, Miot F, Forteza R, Conner GE. Regulated hydrogen peroxide production by Duox in human airway epithelial cells. Am J Respir Cell Mol Biol. 2005;32(5):462-469.
46. Sarr D, Toth E, Gingerich A, Rada B. Antimicrobial actions of dual oxidases and lactoperoxidase. J Microbiol. 2018;56(6):373-386.
47. Rada B, Leto TL. Characterization of hydrogen peroxide production by Duox in bronchial epithelial cells exposed to Pseudomonas aeruginosa. FEBS Lett. 2010;584(5):917-922.
48. Rada B, Lekstrom K, Damian S, Dupuy C, Leto TL. The Pseudomonas toxin pyocyanin inhibits the dual oxidase-based antimicrobial system as it imposes oxidative stress on airway epithelial cells. J Immunol. 2008;181(7):4883-4893.
49. Kim HJ, Kim CH, Kim MJ, Ryu JH, Seong SY, Kim S, Lim SJ, Holtzman MJ, Yoon JH. The Induction of Pattern-Recognition Receptor Expression against Influenza A Virus through Duox2-Derived Reactive Oxygen Species in Nasal Mucosa. Am J Respir Cell Mol Biol. 2015;53(4):525-535.
50. Sarr D, Gingerich AD, Asthiwi NM, Almutairi F, Sautto GA, Ecker J, Nagy T, Kilgore MB, Chandler JD, Ross TM, Tripp RA, Rada B. Dual oxidase 1 promotes antiviral innate immunity. Proc Natl Acad Sci U S A. 2021;118(26).
51. Hsu AP, Korzeniowska A, Aguilar CC, Gu J, Karlins E, Oler AJ, Chen G, Reynoso GV, Davis J, Chaput A, Peng T, Sun L, Lack JB, Bays DJ, Stewart ER, Waldman SE, Powell DA, Donovan FM, Desai JV, Pouladi N, Long Priel DA, Yamanaka D, Rosenzweig SD, Niemela JE, Stoddard J, Freeman AF, Zerbe CS, Kuhns DB, Lussier YA, Olivier KN, Boucher RC, Hickman HD, Frelinger J,

Fierer J, Shubitz LF, Leto TL, Thompson GR, 3rd, Galgiani JN, Lionakis MS, Holland SM. Immunogenetics associated with severe coccidioidomycosis. JCI Insight. 2022;7(22).

52. Ha EM, Oh CT, Bae YS, Lee WJ. A direct role for dual oxidase in Drosophila gut immunity. Science. 2005;310(5749):847-850.

53. Sommer F, Backhed F. The gut microbiota engages different signaling pathways to induce Duox2 expression in the ileum and colon epithelium. Mucosal Immunol. 2015;8(2):372-379.

54. Grasberger H, El-Zaatari M, Dang DT, Merchant JL. Dual oxidases control release of hydrogen peroxide by the gastric epithelium to prevent Helicobacter felis infection and inflammation in mice. Gastroenterology. 2013;145(5):1045-1054.

55. Haberman Y, Tickle TL, Dexheimer PJ, Kim MO, Tang D, Karns R, Baldassano RN, Noe JD, Rosh J, Markowitz J, Heyman MB, Griffiths AM, Crandall WV, Mack DR, Baker SS, Huttenhower C, Keljo DJ, Hyams JS, Kugathasan S, Walters TD, Aronow B, Xavier RJ, Gevers D, Denson LA. Pediatric Crohn disease patients exhibit specific ileal transcriptome and microbiome signature. J Clin Invest. 2014;124(8):3617-3633.

56. Szanto I, Rubbia-Brandt L, Kiss P, Steger K, Banfi B, Kovari E, Herrmann F, Hadengue A, Krause KH. Expression of NOX1, a superoxide-generating NADPH oxidase, in colon cancer and inflammatory bowel disease. J Pathol. 2005;207(2):164-176.

57. Csillag C, Nielsen OH, Vainer B, Olsen J, Dieckgraefe BK, Hendel J, Vind I, Dupuy C, Nielsen FC, Borup R. Expression of the genes dual oxidase 2, lipocalin 2 and regenerating islet-derived 1 alpha in Crohn's disease. Scand J Gastroenterol. 2007;42(4):454-463.

58. Rokutan K, Kawahara T, Kuwano Y, Tominaga K, Nishida K, Teshima-Kondo S. Nox enzymes and oxidative stress in the immunopathology of the gastrointestinal tract. Semin Immunopathol. 2008;30(3):315-327.

59. Parlato M, Charbit-Henrion F, Hayes P, Tiberti A, Aloi M, Cucchiara S, Begue B, Bras M, Pouliet A, Rakotobe S, Ruemmele F, Knaus UG, Cerf-Bensussan N. First Identification of Biallelic Inherited DUOX2 Inactivating Mutations as a

Cause of Very Early Onset Inflammatory Bowel Disease. Gastroenterology. 2017;153(2):609-611 e603.

60. Wesley UV, Bove PF, Hristova M, McCarthy S, van der Vliet A. Airway epithelial cell migration and wound repair by ATP-mediated activation of dual oxidase 1. J Biol Chem. 2007;282(5):3213-3220.
61. Koff JL, Shao MX, Kim S, Ueki IF, Nadel JA. Pseudomonas lipopolysaccharide accelerates wound repair via activation of a novel epithelial cell signaling cascade. J Immunol. 2006;177(12):8693-8700.
62. Gorissen SH, Hristova M, Habibovic A, Sipsey LM, Spiess PC, Janssen-Heininger YM, van der Vliet A. Dual oxidase-1 is required for airway epithelial cell migration and bronchiolar reepithelialization after injury. Am J Respir Cell Mol Biol. 2013;48(3):337-345.
63. Niethammer P, Grabher C, Look AT, Mitchison TJ. A tissue-scale gradient of hydrogen peroxide mediates rapid wound detection in zebrafish. Nature. 2009;459(7249):996-999.
64. Rieger S, Sagasti A. Hydrogen peroxide promotes injury-induced peripheral sensory axon regeneration in the zebrafish skin. PLoS Biol. 2011;9(5):e1000621.
65. Yoo SK, Starnes TW, Deng Q, Huttenlocher A. Lyn is a redox sensor that mediates leukocyte wound attraction in vivo. Nature. 2011;480(7375):109-112.
66. Donko A, Ruisanchez E, Orient A, Enyedi B, Kapui R, Peterfi Z, de Deken X, Benyo Z, Geiszt M. Urothelial cells produce hydrogen peroxide through the activation of Duox1. Free Radic Biol Med. 2010;49(12):2040-2048.
67. Nathan CF. Neutrophil activation on biological surfaces. Massive secretion of hydrogen peroxide in response to products of macrophages and lymphocytes. J Clin Invest. 1987;80(6):1550-1560.
68. Rada B, Boudreau HE, Park JJ, Leto TL. Histamine stimulates hydrogen peroxide production by bronchial epithelial cells via histamine H1 receptor and dual oxidase. Am J Respir Cell Mol Biol. 2014;50(1):125-134.
69. Kwon J, Shatynski KE, Chen H, Morand S, de Deken X, Miot F, Leto TL, Williams MS. The nonphagocytic NADPH oxidase Duox1 mediates a positive feedback loop during T cell receptor signaling. Sci Signal. 2010;3(133):ra59.

70. Bikle DD, Xie Z, Tu CL. Calcium regulation of keratinocyte differentiation. Expert Rev Endocrinol Metab. 2012;7(4):461-472.
71. Choi H, Park JY, Kim HJ, Noh M, Ueyama T, Bae Y, Lee TR, Shin DW. Hydrogen peroxide generated by DUOX1 regulates the expression levels of specific differentiation markers in normal human keratinocytes. J Dermatol Sci. 2014;74(1):56-63.
72. Candi E, Schmidt R, Melino G. The cornified envelope: a model of cell death in the skin. Nat Rev Mol Cell Biol. 2005;6(4):328-340.
73. Edens WA, Sharling L, Cheng G, Shapira R, Kinkade JM, Lee T, Edens HA, Tang X, Sullards C, Flaherty DB, Benian GM, Lambeth JD. Tyrosine cross-linking of extracellular matrix is catalyzed by Duox, a multidomain oxidase/peroxidase with homology to the phagocyte oxidase subunit gp91phox. J Cell Biol. 2001;154(4):879-891.
74. Sirokmany G, Pato A, Zana M, Donko A, Biro A, Nagy P, Geiszt M. Epidermal growth factor-induced hydrogen peroxide production is mediated by dual oxidase 1. Free Radic Biol Med. 2016;97:204-211.
75. Rhee SG, Woo HA, Kil IS, Bae SH. Peroxiredoxin functions as a peroxidase and a regulator and sensor of local peroxides. J Biol Chem. 2012;287(7):4403-4410.
76. Peskin AV, Dickerhof N, Poynton RA, Paton LN, Pace PE, Hampton MB, Winterbourn CC. Hyperoxidation of peroxiredoxins 2 and 3: rate constants for the reactions of the sulfenic acid of the peroxidatic cysteine. J Biol Chem. 2013;288(20):14170-14177.
77. Talagas M, Lebonvallet N, Berthod F, Misery L. Lifting the veil on the keratinocyte contribution to cutaneous nociception. Protein Cell. 2020;11(4):239-250.
78. Lumpkin EA, Caterina MJ. Mechanisms of sensory transduction in the skin. Nature. 2007;445(7130):858-865.
79. Talagas M, Lebonvallet N, Leschiera R, Sinquin G, Elies P, Haftek M, Pennec JP, Ressnikoff D, La Padula V, Le Garrec R, L'Herondelle K, Mignen O, Le Pottier L, Kerfant N, Reux A, Marcorelles P, Misery L. Keratinocytes Communicate with Sensory Neurons via Synaptic-like Contacts. Ann Neurol. 2020;88(6):1205-1219.

80. Xu X, Yu C, Xu L, Xu J. Emerging roles of keratinocytes in nociceptive transduction and regulation. Front Mol Neurosci. 2022;15:982202.
81. Lee H, Caterina MJ. TRPV channels as thermosensory receptors in epithelial cells. Pflugers Arch. 2005;451(1):160-167.
82. Inoue K, Koizumi S, Fuziwara S, Denda S, Inoue K, Denda M. Functional vanilloid receptors in cultured normal human epidermal keratinocytes. Biochem Biophys Res Commun. 2002;291(1):124-129.
83. Mandadi S, Sokabe T, Shibasaki K, Katanosaka K, Mizuno A, Moqrich A, Patapoutian A, Fukumi-Tominaga T, Mizumura K, Tominaga M. TRPV3 in keratinocytes transmits temperature information to sensory neurons via ATP. Pflugers Arch. 2009;458(6):1093-1102.
84. Bang S, Yoo S, Yang TJ, Cho H, Hwang SW. Farnesyl pyrophosphate is a novel pain-producing molecule via specific activation of TRPV3. J Biol Chem. 2010;285(25):19362-19371.
85. Cheng X, Jin J, Hu L, Shen D, Dong XP, Samie MA, Knoff J, Eisinger B, Liu ML, Huang SM, Caterina MJ, Dempsey P, Michael LE, Dlugosz AA, Andrews NC, Clapham DE, Xu H. TRP channel regulates EGFR signaling in hair morphogenesis and skin barrier formation. Cell. 2010;141(2):331-343.
86. Kida N, Sokabe T, Kashio M, Haruna K, Mizuno Y, Suga Y, Nishikawa K, Kanamaru A, Hongo M, Oba A, Tominaga M. Importance of transient receptor potential vanilloid 4 (TRPV4) in epidermal barrier function in human skin keratinocytes. Pflugers Arch. 2012;463(5):715-725.
87. Romero MR, Carroll JM, Watt FM. Analysis of cultured keratinocytes from a transgenic mouse model of psoriasis: effects of suprabasal integrin expression on keratinocyte adhesion, proliferation and terminal differentiation. Exp Dermatol. 1999;8(1):53-67.
88. Tekus V, Horvath A, Hajna Z, Borbely E, Bolcskei K, Boros M, Pinter E, Helyes Z, Petho G, Szolcsanyi J. Noxious heat threshold temperature and pronociceptive effects of allyl isothiocyanate (mustard oil) in TRPV1 or TRPA1 gene-deleted mice. Life Sci. 2016;154:66-74.
89. Ran FA, Hsu PD, Wright J, Agarwala V, Scott DA, Zhang F. Genome engineering using the CRISPR-Cas9 system. Nat Protoc. 2013;8(11):2281-2308.

90. Lowe O, Rezende F, Heidler J, Wittig I, Helfinger V, Brandes RP, Schroder K. BIAM switch assay coupled to mass spectrometry identifies novel redox targets of NADPH oxidase 4. Redox Biol. 2019;21:101125.
91. Pato A, Bolcskei K, Donko A, Kaszas D, Boros M, Bodrogi L, Varady G, Pape VFS, Roux BT, Enyedi B, Helyes Z, Watt FM, Sirokmany G, Geiszt M. Hydrogen peroxide production by epidermal dual oxidase 1 regulates nociceptive sensory signals. Redox Biol. 2023;62:102670.
92. Wu Z, He K, Chen Y, Li H, Pan S, Li B, Liu T, Xi F, Deng F, Wang H, Du J, Jing M, Li Y. A sensitive GRAB sensor for detecting extracellular ATP in vitro and in vivo. Neuron. 2022;110(5):770-782 e775.
93. Stringer C, Wang T, Michaelos M, Pachitariu M. Cellpose: a generalist algorithm for cellular segmentation. Nat Methods. 2021;18(1):100-106.
94. Bae YS, Kang SW, Seo MS, Baines IC, Tekle E, Chock PB, Rhee SG. Epidermal growth factor (EGF)-induced generation of hydrogen peroxide. Role in EGF receptor-mediated tyrosine phosphorylation. J Biol Chem. 1997;272(1):217-221.
95. Villalobo A, Ruano MJ, Palomo-Jiménez PI, Li H, Martín-Nieto J. The Epidermal Growth Factor Receptor and the Calcium Signal. In: Pochet R, Donato R, Haiech J, Heizmann C, Gerke V, editors. Calcium: The Molecular Basis of Calcium Action in Biology and Medicine. Dordrecht: Springer Netherlands; 2000. p. 287-303.
96. Goldman R, Moshonov S, Zor U. Generation of reactive oxygen species in a human keratinocyte cell line: role of calcium. Arch Biochem Biophys. 1998;350(1):10-18.
97. Rhee SG, Chang TS, Bae YS, Lee SR, Kang SW. Cellular regulation by hydrogen peroxide. J Am Soc Nephrol. 2003;14(8 Suppl 3):S211-215.
98. Tonks NK. Redox redux: revisiting PTPs and the control of cell signaling. Cell. 2005;121(5):667-670.
99. Lee SR, Kwon KS, Kim SR, Rhee SG. Reversible inactivation of protein-tyrosine phosphatase 1B in A431 cells stimulated with epidermal growth factor. J Biol Chem. 1998;273(25):15366-15372.

100. McNamara CR, Mandel-Brehm J, Bautista DM, Siemens J, Deranian KL, Zhao M, Hayward NJ, Chong JA, Julius D, Moran MM, Fanger CM. TRPA1 mediates formalin-induced pain. Proc Natl Acad Sci U S A. 2007;104(33):13525-13530.
101. Larios JM, Budhiraja R, Fanburg BL, Thannickal VJ. Oxidative protein cross-linking reactions involving L-tyrosine in transforming growth factor-beta1-stimulated fibroblasts. J Biol Chem. 2001;276(20):17437-17441.
102. Kamath RS, Fraser AG, Dong Y, Poulin G, Durbin R, Gotta M, Kanapin A, Le Bot N, Moreno S, Sohrmann M, Welchman DP, Zipperlen P, Ahringer J. Systematic functional analysis of the Caenorhabditis elegans genome using RNAi. Nature. 2003;421(6920):231-237.
103. Caterina MJ, Julius D. Sense and specificity: a molecular identity for nociceptors. Curr Opin Neurobiol. 1999;9(5):525-530.
104. Mizumoto N, Mummert ME, Shalhevet D, Takashima A. Keratinocyte ATP release assay for testing skin-irritating potentials of structurally diverse chemicals. J Invest Dermatol. 2003;121(5):1066-1072.
105. Moehring F, Cowie AM, Menzel AD, Weyer AD, Grzybowski M, Arzua T, Geurts AM, Palygin O, Stucky CL. Keratinocytes mediate innocuous and noxious touch via ATP-P2X4 signaling. Elife. 2018;7.
106. Koizumi S, Fujishita K, Inoue K, Shigemoto-Mogami Y, Tsuda M, Inoue K. Ca2+ waves in keratinocytes are transmitted to sensory neurons: the involvement of extracellular ATP and P2Y2 receptor activation. Biochem J. 2004;380(Pt 2):329-338.
107. Tsutsumi M, Inoue K, Denda S, Ikeyama K, Goto M, Denda M. Mechanical-stimulation-evoked calcium waves in proliferating and differentiated human keratinocytes. Cell Tissue Res. 2009;338(1):99-106.
108. Goto M, Ikeyama K, Tsutsumi M, Denda S, Denda M. Calcium ion propagation in cultured keratinocytes and other cells in skin in response to hydraulic pressure stimulation. J Cell Physiol. 2010;224(1):229-233.
109. Huang SM, Lee H, Chung MK, Park U, Yu YY, Bradshaw HB, Coulombe PA, Walker JM, Caterina MJ. Overexpressed transient receptor potential vanilloid 3 ion channels in skin keratinocytes modulate pain sensitivity via prostaglandin E2. J Neurosci. 2008;28(51):13727-13737.

110. Peier AM, Reeve AJ, Andersson DA, Moqrich A, Earley TJ, Hergarden AC, Story GM, Colley S, Hogenesch JB, McIntyre P, Bevan S, Patapoutian A. A heat-sensitive TRP channel expressed in keratinocytes. Science. 2002;296(5575):2046-2049.
111. Guler AD, Lee H, Iida T, Shimizu I, Tominaga M, Caterina M. Heat-evoked activation of the ion channel, TRPV4. J Neurosci. 2002;22(15):6408-6414.
112. Chung MK, Lee H, Mizuno A, Suzuki M, Caterina MJ. TRPV3 and TRPV4 mediate warmth-evoked currents in primary mouse keratinocytes. J Biol Chem. 2004;279(20):21569-21575.
113. Sies H. Hydrogen peroxide as a central redox signaling molecule in physiological oxidative stress: Oxidative eustress. Redox Biol. 2017;11:613-619.
114. Manteniotis S, Lehmann R, Flegel C, Vogel F, Hofreuter A, Schreiner BS, Altmuller J, Becker C, Schobel N, Hatt H, Gisselmann G. Comprehensive RNA-Seq expression analysis of sensory ganglia with a focus on ion channels and GPCRs in Trigeminal ganglia. PLoS One. 2013;8(11):e79523.
115. Mahmoud O, Soares GB, Yosipovitch G. Transient Receptor Potential Channels and Itch. Int J Mol Sci. 2022;24(1).
116. Gamper N, Zaika O, Li Y, Martin P, Hernandez CC, Perez MR, Wang AY, Jaffe DB, Shapiro MS. Oxidative modification of M-type K(+) channels as a mechanism of cytoprotective neuronal silencing. EMBO J. 2006;25(20):4996-5004.
117. Jin H, Heller DA, Kalbacova M, Kim JH, Zhang J, Boghossian AA, Maheshri N, Strano MS. Detection of single-molecule H2O2 signalling from epidermal growth factor receptor using fluorescent single-walled carbon nanotubes. Nat Nanotechnol. 2010;5(4):302-309.
118. Dickinson BC, Huynh C, Chang CJ. A palette of fluorescent probes with varying emission colors for imaging hydrogen peroxide signaling in living cells. J Am Chem Soc. 2010;132(16):5906-5915.
119. Paulsen CE, Truong TH, Garcia FJ, Homann A, Gupta V, Leonard SE, Carroll KS. Peroxide-dependent sulfenylation of the EGFR catalytic site enhances kinase activity. Nat Chem Biol. 2011;8(1):57-64.

120. Yang XH, Man XY, Cai SQ, Yao YG, Bu ZY, Zheng M. Expression of VEGFR-2 on HaCaT cells is regulated by VEGF and plays an active role in mediating VEGF induced effects. Biochem Biophys Res Commun. 2006;349(1):31-38.
121. Wraight CJ, Werther GA. Insulin-like growth factor-I and epidermal growth factor regulate insulin-like growth factor binding protein-3 (IGFBP-3) in the human keratinocyte cell line HaCaT. J Invest Dermatol. 1995;105(4):602-607.
122. Miller EW, Dickinson BC, Chang CJ. Aquaporin-3 mediates hydrogen peroxide uptake to regulate downstream intracellular signaling. Proc Natl Acad Sci U S A. 2010;107(36):15681-15686.
123. Lu J, Holmgren A. The thioredoxin antioxidant system. Free Radic Biol Med. 2014;66:75-87.
124. Sobotta MC, Liou W, Stocker S, Talwar D, Oehler M, Ruppert T, Scharf AN, Dick TP. Peroxiredoxin-2 and STAT3 form a redox relay for H2O2 signaling. Nat Chem Biol. 2015;11(1):64-70.
125. Boots AW, Hristova M, Kasahara DI, Haenen GR, Bast A, van der Vliet A. ATP-mediated activation of the NADPH oxidase DUOX1 mediates airway epithelial responses to bacterial stimuli. J Biol Chem. 2009;284(26):17858-17867.
126. Hristova M, Habibovic A, Veith C, Janssen-Heininger YM, Dixon AE, Geiszt M, van der Vliet A. Airway epithelial dual oxidase 1 mediates allergen-induced IL-33 secretion and activation of type 2 immune responses. J Allergy Clin Immunol. 2016;137(5):1545-1556 e1511.
127. Allaoui A, Botteaux A, Dumont JE, Hoste C, De Deken X. Dual oxidases and hydrogen peroxide in a complex dialogue between host mucosae and bacteria. Trends Mol Med. 2009;15(12):571-579.
128. Denda M, Nakanishi S. Do epidermal keratinocytes have sensory and information processing systems? Exp Dermatol. 2022;31(4):459-474.
129. Otsubo Y, Satoh Y, Kodama M, Araki Y, Satomoto M, Sakamoto E, Pages G, Pouyssegur J, Endo S, Kazama T. Mechanical allodynia but not thermal hyperalgesia is impaired in mice deficient for ERK2 in the central nervous system. Pain. 2012;153(11):2241-2252.

130. Ansel J, Perry P, Brown J, Damm D, Phan T, Hart C, Luger T, Hefeneider S. Cytokine modulation of keratinocyte cytokines. J Invest Dermatol. 1990;94(6 Suppl):101S-107S.
131. Andoh T, Katsube N, Maruyama M, Kuraishi Y. Involvement of leukotriene B(4) in substance P-induced itch-associated response in mice. J Invest Dermatol. 2001;117(6):1621-1626.
132. Burrell HE, Wlodarski B, Foster BJ, Buckley KA, Sharpe GR, Quayle JM, Simpson AW, Gallagher JA. Human keratinocytes release ATP and utilize three mechanisms for nucleotide interconversion at the cell surface. J Biol Chem. 2005;280(33):29667-29676.
133. Bigliardi PL, Tobin DJ, Gaveriaux-Ruff C, Bigliardi-Qi M. Opioids and the skin--where do we stand? Exp Dermatol. 2009;18(5):424-430.
134. Andersson DA, Gentry C, Moss S, Bevan S. Transient receptor potential A1 is a sensory receptor for multiple products of oxidative stress. J Neurosci. 2008;28(10):2485-2494.
135. Wang ZQ, Porreca F, Cuzzocrea S, Galen K, Lightfoot R, Masini E, Muscoli C, Mollace V, Ndengele M, Ischiropoulos H, Salvemini D. A newly identified role for superoxide in inflammatory pain. J Pharmacol Exp Ther. 2004;309(3):869-878.
136. Salvemini D, Little JW, Doyle T, Neumann WL. Roles of reactive oxygen and nitrogen species in pain. Free Radic Biol Med. 2011;51(5):951-966.

9. Bibliography of the candidate's publications

Candidate's publications related to the thesis:

Pató A, Bölcskei K, Donkó Á, Kaszás D, Boros M, Bodrogi L, Várady G, Pape VFS, Roux BT, Enyedi B, Helyes Z, Watt FM, Sirokmány G, Geiszt M. *Hydrogen peroxide production by epidermal dual oxidase 1 regulates nociceptive sensory signals.* Redox Biol. 2023 doi: 10.1016/j.redox.2023.102670

Sirokmány G, **Pató A**, Zana M, Donkó Á, Bíró A, Nagy P, Geiszt M. *Epidermal growth factor-induced hydrogen peroxide production is mediated by dual oxidase 1.* Free Radic Biol Med. 2016 doi: 10.1016/j.freeradbiomed.2016.05.028

Candidate's publications unrelated to the thesis:

Scherr AL, Jassowicz A, **Pató A**, Elssner C, Ismail L, Schmitt N, Hoffmeister P, Neukirch L, Gdynia G, Goeppert B, Schulze-Bergkamen H, Jäger D, Köhler BC. *Knockdown of Atg7 Induces Nuclear-LC3 Dependent Apoptosis and Augments* Chemotherapy in Colorectal Cancer Cells. Int J Mol Sci. 2020
doi: 10.3390/ijms21031099

Birtalan E, Danos K, Gurbi B, Brauswetter D, Halasz J, Kalocsane Piurko V, Acs B, Antal B, Mihalyi R, **Pato A**, Fent Z, Polony G, Timar J, Tamas L. *Expression of PD-L1 on Immune Cells Shows Better Prognosis in Laryngeal, Oropharygeal, and Hypopharyngeal Cancer.* Appl Immunohistochem Mol Morphol. 2018
doi: 10.1097/PAI.0000000000000590

Dános K, Brauswetter D, Birtalan E, **Pató A**, Bencsik G, Krenács T, Peták I, Tamás L. *The Potential Prognostic Value of Connexin 43 Expression in Head and Neck Squamous Cell Carcinomas.* Appl Immunohistochem Mol Morphol. 2016
doi: 10.1097/PAI.0000000000000212

10. Acknowledgements

I would like to express my deepest gratitude towards my supervisor, Dr. Gábor Sirokmány, who has been an invaluable mentor throughout my journey as a TDK student and later as a Ph.D. student. I am truly grateful for his guidance and unwavering support.
I want to express my genuine appreciation to Prof. Miklós Geiszt for the opportunity to work in his laboratory. His expert guidance and invaluable professional advice have helped me overcome many challenges. The atmosphere of his laboratory is conducive to learning and growth, and I am truly grateful for the opportunities he has afforded me.
I would also like to thank Prof. László Hunyady and Prof. Attila Mócsai, the heads of the Department of Physiology, and Prof. Péter Enyedi, the chairman of the Molecular Medicine Doctoral School, for giving me the opportunity to research and complete my dissertation.
I would also like to express my sincere gratitude to Dr. Lilla Bodrogi, Dr. Balázs Enyedi and his laboratory, Prof. Zsuzsanna Helyes and her laboratory, and Dr. György Várady. Their expertise and knowledge have been invaluable to my research, and I am grateful for their help.
I am indebted to my colleagues in the Department of Physiology, and I would especially like to thank current and former laboratory members, namely Dr. Ágnes Donkó, Dr. Hajnal Anna Kovács, Dr. Veronika F. S. Pape, Dr. Gábor Petheő, Zsolt Szeles, and Dr. Bernadett Éva Balázs Trencsényiné for their guidance, support, and encouragement. I would also like to extend my gratitude to Barbara Bodor-Kis, Beáta Molnár, and Regina Tóth-Kun for their technical assistance. I would also like to give special thanks to laboratory animal care workers Szabina Kravecz and Ádám Marinkás.
Finally, I would like to express my appreciation to my family and friends for their continuous and unconditional support throughout my Ph.D. studies.